SEDIMENTOLOGY the journal of the International Association of Sedimentologists

Sedimentology (2020) **67**, 1973–2012 doi: 10.1111/sed.12692

Late Palaeozoic red beds elucidate fluvial architectures preserving large woody debris in the seasonal tropics of central Pangaea

STEFFEN TRÜMPER*‡, BIRGIT GAITZSCH†, JÖRG W. SCHNEIDER‡§, BODO-CARLO EHLING¶, REINHARD KLEEBERG** and RONNY RÖßLER*‡

**Museum für Naturkunde Chemnitz, Moritzstraße 20, D-09111 Chemnitz, Germany (E-mail: steffen.truemper@hotmail.de)*

†Geowissenschaftliche Sammlungen, TU Bergakademie Freiberg, Bernhard-von-Cotta-Straße 2, D-09599 Freiberg, Germany

‡Institut für Geologie, TU Bergakademie Freiberg, Bernhard-von-Cotta-Straße 2, D-09599 Freiberg, Germany

§Institute of Geology and Petroleum Technologies, Kazan Federal University, Kremlyovskaya 18, 420008 Kazan, Russia

¶Landesamt für Geologie und Bergwesen Sachsen-Anhalt, Köthener Straße 38, D-06118 Halle (Saale), Germany

***Institut für Mineralogie, TU Bergakademie Freiberg, Brennhausgasse 14, D-09599 Freiberg, Germany*

Associate Editor – Christopher Fielding

ABSTRACT

Fluvial red beds containing anatomically preserved large woody debris shed new light on seasonally dry biomes of the Pennsylvanian–Permian transition and elucidate the concurrence of river depositional systems and vegetation. As a result, the occurrence, distribution and preservation of petrified large woody debris accumulations are considered crucial to understanding the role of arborescent vegetation in shaping fluvial environments. This study reports sizeable silicified trunks and corresponding fluvial architectures from the uppermost Pennsylvanian (upper Gzhelian) Siebigerode Formation (Kyffhäuser, central Germany). The origin, taphonomy and depositional environment of the fossil woods are elucidated by using a multidisciplinary approach including geological mapping, lithofacies analysis, sediment petrography, wood anatomical studies and microstructure analyses. Results reflect the gradual burial of a gentle basement elevation by sand-bed to gravel-bed braided rivers at the northwestern margin of the perimontane Saale Basin. Facies architectures resulted from a complex interplay of syndepositional tectonics, repeated palaeorelief rejuvenation, high-frequency channel avulsion, seasonally dry climate and woody debris–sediment interactions. The alluvial influx and cut-bank erosion recruited trunks from adjacent semi-riparian slope habitats vegetated by up to 40 m tall cordaitaleans and conifers. High discharge in wide braids facilitated uncongested transport of large woody debris. Trunk entombment and initial preservation resulted from grounding on barforms, anchoring by attached roots and subsequent burial. The post-depositional two-phase silicification was influenced by hydrothermal hematite mineralization and determined a selective wood preservation pattern known as 'pointstone'. Large woody debris-induced sedimentary structures ('LWDISS') are introduced as a class of sediment structures formed by the biogenic impact on terrestrial deposition.

Keywords Braided river, facies analysis, Pennsylvanian, petrified wood, seasonality, silicification.

INTRODUCTION

Compared to the common clastic load, large woody debris (LWD) represents an exceptional component in fluvial systems. Favoured by its elongated or branching geometry, floating wood may clog active channels and, thus, initiates scouring, bank erosion, channel avulsion and incision (Gastaldo & Degges, 2007; Gibling *et al.*, 2010). Log jams and other plant debris also play a constructive role because they trigger bar formation, stabilize cut banks or form frameworks, upon which fluvial islands may evolve (Abbe & Montgomery, 1996; Fielding *et al.*, 1997; Alexander *et al.*, 1999). Large woody debris hence crucially shapes river morphology and impacts the resulting lithofacies patterns.

Fossil log jams of Pennsylvanian age have received increasing scientific attention in the past 20 years, because they shed light on the riparian and basin-marginal vegetation of seasonally dry environments in equatorial Pangaea (Falcon-Lang & Scott, 2000; Falcon-Lang & Bashforth, 2004; Bashforth *et al.*, 2014). Previous studies, however, focused on LWD provenance and source area palaeoecology, albeit relatively little is known about the constraints determining wood entombment and fossilization in ancient fluvial systems (Alexander *et al.*, 1999; Fielding & Alexander, 2001). This assessment also includes the interaction of LWD and sediments, which is well-studied in modern rivers and flume experiments (Keller & Swanson, 1979; Abbe & Montgomery, 1996, 2003; Fielding & Alexander, 1996; Wallerstein *et al.*, 2001; Nakayama *et al.*, 2002) but still poorly understood in the geological record (Fielding & Alexander, 2001; Ielpi *et al.*, 2014).

Pennsylvanian strata exposed in the Kyffhäuser, central Germany, represent one of the largest occurrences of petrified wood by volume from the late Palaeozoic of the Northern Hemisphere. Up to 20 m long logs are embedded individually and horizontally in fluvial deposits pointing to transport as LWD. Extensive sandstone quarrying over recent centuries has generated numerous exposures, which provide the chance to study the three-dimensional relations of petrified woods and fluvial architecture. The aims of this study are for the factors influencing the origin, occurrence and entombment of LWD in the Kyffhäuser to be elucidated, including a description and evaluation of the corresponding large woody debris-induced sedimentary structures (LWDISS). Results will be discussed against the background to reconstruct the depositional environment, including its evolution and vegetation through time and space.

GEOLOGICAL BACKGROUND

Regional geology and stratigraphy

The Kyffhäuser represents an up to 474 m elevation in central Germany located at the border of the federal states of Thuringia and Saxony-Anhalt (Fig. 1A). Structurally, this elevation is formed by a south-tilting fault block, which has been uplifted by 1·5 km along the Kyffhäuser and Kelbra faults since the Late Cretaceous (Schriel & Fulda, 1926a; Zeh *et al.*, 2005; Franzke *et al.*, 2007). Accordingly, Variscan basement rocks of the Kyffhäuser Crystalline Complex are exposed within a 1·5 km^2 area along the northern margin of the Kyffhäuser (Fig. 1A). To the south, the basement is concealed by an approximately 700 m thick succession of south-dipping siliciclastic strata of the uppermost Pennsylvanian (Stephanian C) Siebigerode Formation (Schriel & Fulda, 1926a,b; Trümper, 2013). Separated by an angular unconformity encompassing a hiatus of *ca* 39 million years (Schriel & Fulda, 1926b; Schneider *et al.*, 2015), the Siebigerode Formation is overlain by uppermost Permian sedimentary strata of the continental Upper Rotliegend Eisleben Formation and, finally, the marine–evaporitic Zechstein Group (Fig. 1A).

During the Late Pennsylvanian, the Kyffhäuser area occupied a basin-marginal position at the north-western flank of the north-east/south-west trending Saale Basin (Fig. 1C). Named after the modern Saale River, it was formed on the tectonically inverted Mid-German Crystalline Zone as a consequence of uprising crustal extension in Central Europe from 305 Ma onward (Schneider *et al.*, 2005; Kroner & Romer, 2013). Owing to a perimontane position at the northern margin of the Variscan Mountain Chain (Fig. 1B), the Saale Basin was part of a drainage system connecting the Bohemian basins with the Variscan Foreland Basin (Schneider & Zajic, 1994; Gaitzsch *et al.*, 1998). Deposition occurred under seasonally dry, tropical conditions, as recorded by palaeosols (Calcisols and Vertisols), lacustrine carbonates and alluvial fan to braided river sediments (Schneider *et al.*, 2005). Although located at 10° northern latitude (Fig. 1B), such a climate was favoured by the

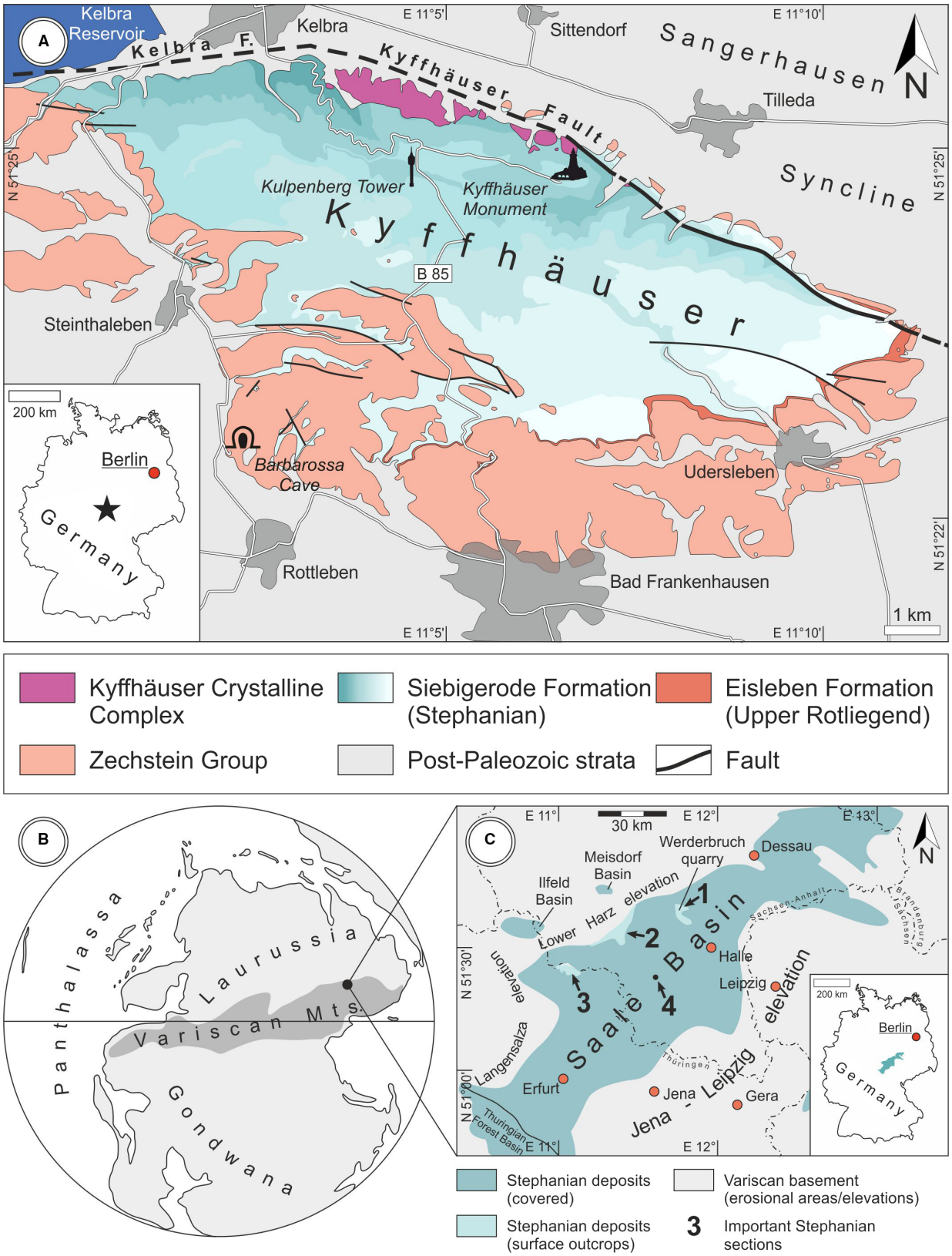

Fig. 1. Geological map of the Kyffhäuser (A) and palaeogeography of the Saale Basin (B) and (C). Surface outcrops: 1 – Saale River valley near Wettin; 2 – South-east Harz Foreland; 3 – Kyffhäuser; 4 – well Querfurt 1/64. Compiled and modified after Schriel & von Bülow (1925, 1926) and Schneider *et al.* (2005).

orientation of the basin perpendicular to prevailing wind directions (Gebhardt & Hiete, 2013).

Kasimovian to Gzhelian (Stephanian) strata of the Saale Basin are assigned to the Mansfeld Subgroup, with the up to 800 m thick Siebigerode Formation being the uppermost lithostratigraphic unit (Fig. 2; Schneider *et al.*, 1995). The latter was formed during the late Gzhelian under more humid conditions of the inter-regionally traceable wet phase B (Fig. 2). Lithofacies of the Siebigerode Formation are characterized by red beds deposited by predominantly sand-bed braided rivers and associated floodplains in a vast alluvial plain (Schneider *et al.*, 2005). In the basin centre, a greyish succession of palustrine, lacustrine and fluvial origin is referred to as the Wettin Member, which hosts a diverse adpression flora derived from lycopsids, calamitaleans, ferns, pteridosperms, cordaitaleans and conifers (Beyschlag & Fritsch, 1888; Remy *et al.*, 1961; Barthel *et al.*, 1975). The Siebigerode Formation expanded deposition to the basin margins and was the first lithostratigraphic unit of the Mansfeld Subgroup to reach the Kyffhäuser area (Trümper, 2013). Based on fossil insects and amphibians from lacustrine strata of the Wettin Member, the Siebigerode Formation is assigned to the *Syscioblatta dohrni–Sysciophlebia euglyptica* and the *Branchiosaurus saalensis–Apateon intermedius* biozones (Stephanian C; Schneider, 1996; Schneider & Werneburg, 2012). Uranium–lead (U-Pb) ages from laccolites of the Halle Volcanic Complex which intruded into the still unconsolidated Siebigerode Formation indicate a minimum age of deposition of 300 Ma (Breitkreuz & Kennedy, 1999; Ehling *et al.*, 2005; Breitkreuz *et al.*, 2009). This is supported by a U-Pb age of $299 \pm 3{\cdot}2$ Ma gained from a tuff bed near the top of the Siebigerode Formation in the Kyffhäuser (Trümper, 2013).

The Siebigerode Formation at the Kyffhäuser

The knowledge of the structure and stratigraphy of the Kyffhäuser section has developed mainly in the 20th century owing to field mapping by Schriel & von Bülow (1925, 1926) and comprehensive petrographic studies in the 1950s to 1970s (Ludwig, 1955; Hoyningen-Huene, 1960; Meissner, 1963; Meister, 1967; Schirmer, 1975). Because uplift and tilting of the Kyffhäuser Block also involved gentle folding, the youngest Stephanian strata are found north of Udersleben (Fig. 1A). However, the Siebigerode Formation displays a cyclic structure comprising ten 20 to 150 m thick sandy to gravelly units (units a to k) interbedded with eight fine-clastic units ($ß_1$ to $ß_8$) – a structure and terminology introduced by Schriel & von Bülow (1925, 1926) and confirmed and, thus, adopted in this study (Fig. 2). The pale red sandstones consist of quartz (40 to 70 vol%), quartzite (2 to 40 vol%) and intraclasts (siltstones, fine-grained sandstones, 0 to 25 vol%; Meister, 1967; Schirmer, 1975). The content of the latter is highest in unit b. Other lithic components (igneous rock clasts, phyllites and slates) occur rarely with magmatite clasts being most abundant but still accessory in the uppermost unit c (Schirmer, 1975). Feldspars appear from unit g onward but do not exceed 18 vol%. Based on detrital mineralogy provided by Schirmer (1975), the Kyffhäuser sandstones predominantly represent sublitharenites following the classification of McBride (1963) and, thus, possibly point to a recycled-orogen source (Dickinson, 1985). In unit k, minor subarkoses to arkoses occur. Intergranular space accounting for 2 to 26 vol% of the rocks is filled by kaolin-group minerals, calcite and hematite. According to Schirmer (1975), the heavy-mineral association is of low diversity and comprises zircon, tourmaline and rutile. Based on lithics and palaeocurrent data (Schirmer, 1975), sediments of the lower units a and b were provided by source areas in the north-west. Starting with unit c, clastic material derived from basement uplifts in south-western to south-eastern directions.

MATERIALS AND METHODS

Facies analysis

Within the scope of this study, 182 outcrops in the Kyffhäuser (quarries, rock spurs, cliffs, temporary exposures, construction areas and slopes along streets) were documented with respect to their lithofacies architecture. Following the hierarchical facies analysis concept proposed by Miall (1977, 2006), lithofacies types (LFTs) as the smallest building blocks of fluvial lithofacies architecture have been characterized according to their texture, structure, thickness and lateral extent. Each LFT is abbreviated by a combination of a capital letter representing the dominant grain size followed by one or two small letters reflecting the structure (see Table 1). The LFTs occur in different combinations, which possess

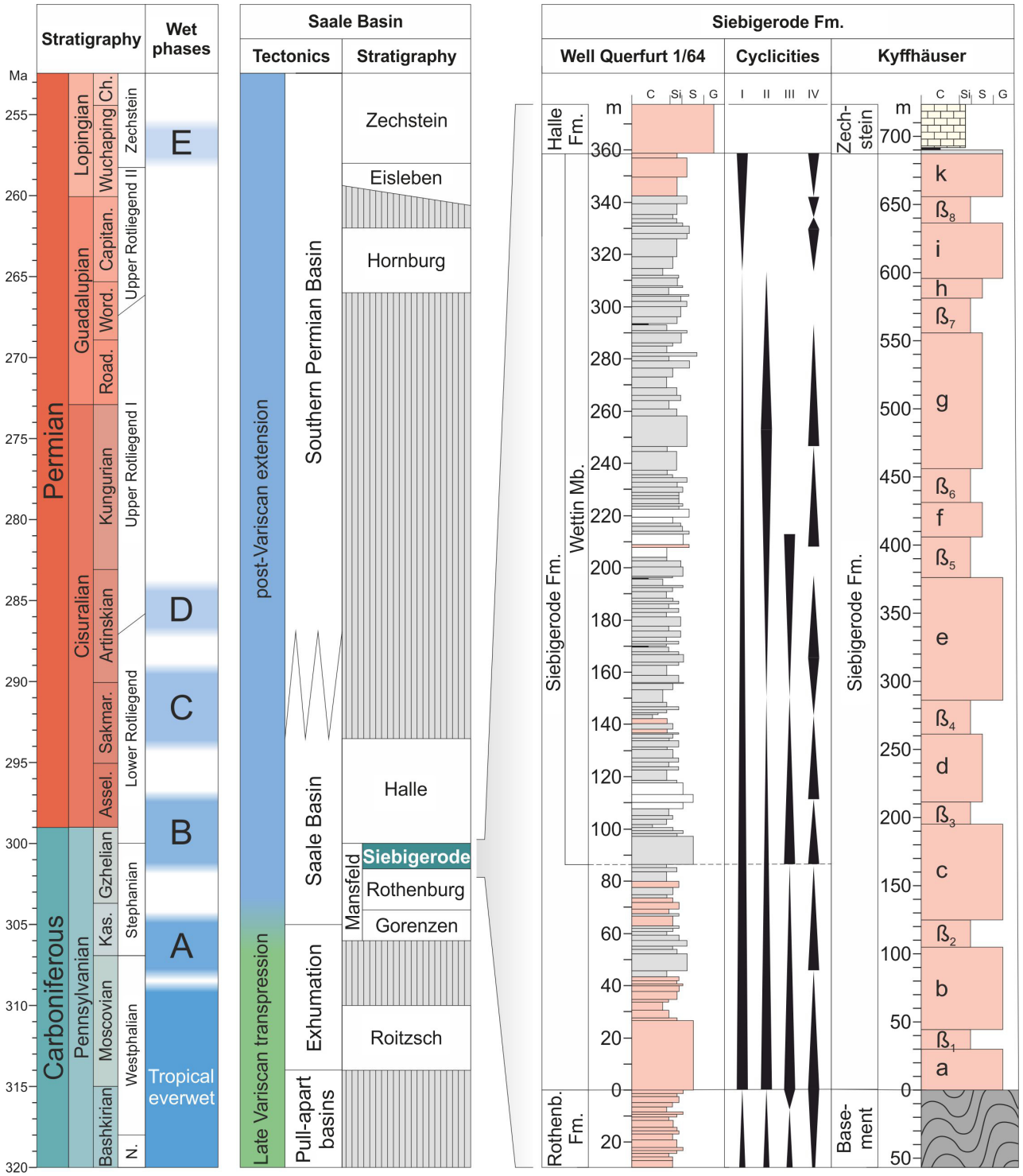

Fig. 2. Stratigraphy of the Saale Basin and the Siebigerode Formation. The latter is shown with one profile in the basin centre (well Querfurt 1/64) and the basin-marginal Kyffhäuser (for positions of both see Fig. 1C). Colouration is based upon rock colour. White units represent areas of lost cores which were lithologically identified via gamma-ray logging. Summarized and modified after Schriel & Fulda (1926a,b), Roscher & Schneider (2006), Schneider *et al.* (2006), Gebhardt & Hiete (2013), Kroner & Romer (2013) and Schneider *et al.* (2015).

Table 1. Lithofacies type code (modified after Miall, 2006).

Capital letter	Lower case letter
Grain size	**Bedding**
G: Gravel	m: massive
S: Sand	r: ripple cross-bedded
F: Fine-clastics	p: planar cross-bedded
	t: trough cross-bedded
	l: low-angle cross-bedded
	h: horizontally-bedded
	i: inverse-gradedim: imbricated
Special	**Special**
P: Palaeosol	b: bioturbated
	ro: rooted
	v: vertic
	c: calcic
	cm: clast-supported, massive
	mm: matrix-supported, massive

specific geometries and will be called lithofacies associations (LFA) hereafter. Each LFA is named according to the dominant architectural element/s. The stratigraphic occurrence of the LFAs was mapped along six transects. Lateral correlation of the resulting eight profiles is used to describe lithofacies architecture and the evolution of the fluvial system through time and space. Stratigraphic correlation rests upon lithostratigraphic and cyclostratigraphic criteria: distinctive lithological features of floodplain and coarse-clastic units (palaeosol maturity, bioturbation intensity, lithofacies architectures and kaolin content), which can be traced across the sections in the field, and large-scale cycles and trends in the Kyffhäuser section (i.e. fining-upward cycles). Azimuthal diagrams showing palaeocurrent data are corrected with respect to post-depositional tilting. The latter was estimated across the Kyffhäuser area by measuring sedimentary structures of which an originally horizontal orientation can be assumed (upper plane bed sandstones, horizontally bedded fine-clastics, even and horizontal bases of non-erosive barforms and bedforms).

Clay mineralogy and cathodoluminescence microscopy

Like the embedding rocks, fossil wood undergoes sedimentary diagenesis, which may support or overprint and, thus, constrain the mineralization process. In this study, sediment petrography was characterized by using 10 covered thin sections (28 × 48 mm) complemented by clay mineral and cathodoluminescence (CL) analyses. Descriptions of mineral composition were carried out under plane-polarized (PPL) and cross-polarized transmitted light (XPL) using a Zeiss Axiolab microscope attached to an Axiocam ERc 5s camera (Carl Zeiss AG, Oberkochen, Germany). The identification of intergranular clay minerals was performed by X-ray diffraction on two samples from the Kyffhäuser and the Saale River valley (Fig. 1C, base of the Siebigerode Formation at the Werderbruch quarry near Rothenburg; 51°38′06·8″N, 11°45′28·7″E). The analysis is based on *ca* 20 to 30 mg from each sample separated manually with a preparation needle. The powder was mixed with a drop of ethanol and prepared on a Si low background sample holder in a thin layer or a small cavity, without pressing, for a minimum of preferred orientation. Diffraction patterns were measured in the angular range of 5° to 80° 2Θ in constant sample area mode with Co Kα radiation on a URD-6 Bragg-Brentano diffractometer (Seifert FPM GmbH, Freiberg, Germany), equipped with a Si-drift detector Meteor0D. Polytype interpretation was undertaken based on the ICDD PDF-4+ database, issue 2016. The CL analyses were carried out on polished thin sections (28 × 48 mm) coated with carbon to prevent any build-up of electrical charge. The CL microscope was a 'hot cathode' CL microscope HC1-LM (designed by U. Zinkernagel and modified by R. Neuser at the Ruhr-University, Bochum, Germany), which used an acceleration voltage of 14 kV and a beam current of 0·2 mA. Cathodoluminescence images were taken with an Olympus DP72 digital camera (Olympus Corporation, Tokyo, Japan). An Acton Research SP-2356 spectrograph (Princeton Instruments, Acton, MA, USA) was linked to the microscope via an optical glass-fibre guide and served for recording CL spectra in the wavelength range of 370 to 900 nm under standardized conditions. The measurement spot size of 30 μm in diameter was assured by a pinhole aperture. An Hg-halogen lamp ensured wavelength calibration. Due to the light diffraction, measured spectra represent interferences of different CL signals.

Palaeobotany

In order to characterize the structure and site-specific conditions of the forests providing LWD, plant anatomical studies were carried out on 53 three-dimensionally preserved petrified-log specimens. Systematic identification is based on characterizing wood and pith anatomy from

thin sections in radial–longitudinal, tangential–longitudinal and transverse directions, as well as descriptions of branching patterns from cut and unprocessed specimens. Tree rings are presumed to shed light on water availability, climate seasonality or incisive events (droughts and diseases) and their thickness and structure were documented. Descriptions were carried out by using NIS-Elements D software version 3.2 under a Nikon SMZ 1500 binocular microscope (Nikon, Tokyo, Japan). Photographs were taken with a Nikon D5300 digital camera. Investigated specimens belong to the private collection of Matthias Borchardt, Steinthaleben (BS) and six public collections – Museum für Naturkunde Chemnitz (MfNC), Regionalmuseum Bad Frankenhausen (RMBF), Naturhistorisches Museum Schleusingen (NMS), Museum für Naturkunde Berlin, Naturhistorisches Museum Rudolstadt and Palaeontological collection of the TU Bergakademie Freiberg. Calculations of wood compaction and estimations of original tree height are based on 19 petrified logs with complete to almost complete diameter mounted upright in gardens and along streets in the Kyffhäuser region, or still remaining *in situ* in outcrops. The extent of wood compaction is expressed as the degree to which a circular trunk transverse section has been modified to an elliptical one during compression of a horizontal log (in per cent). Such deformation is based upon compactional (oblate) strain resulting in reductions of vertical but not horizontal diameters (Fossen, 2016). Hence, the horizontal diameter (d_h) equals the original vertical diameter (d_0). The degree of wood compaction is calculated as follows:

$$\Delta d[\%] = \frac{d_v}{d_0} \times 100\% = \frac{d_v}{d_h} \times 100\%$$

where Δd is the degree of wood compaction, d_v the measured vertical diameter, d_0 the original vertical diameter, and d_h the horizontal diameter. Calculation of original tree height h rests upon the empirical formula provided by Niklas (1994):

$$h[m] = 10^{(1{\cdot}59 + 0{\cdot}39 \times \log_{10}(d_h[m]))}$$

This equation usually requires the trunk diameter to be measured 1·3 m above ground level. Because all of the trunks in the Kyffhäuser section were transported and fragmented, most calculations provide minimum values for the original tree height. In two samples, which represent ground-level parts of trunks, the original tree height is approximated by the calculated values.

LITHOFACIES ANALYSIS

Lithofacies types

Facies analysis revealed 15 siliciclastic LFTs, of which three are fine-clastic (Fig. 3A to C), five are sandy (Fig. 3D to J) and seven are gravelly (Fig. 4; for a brief description of all LFTs see Table 2). The maximum clast size in the Kyffhäuser section is 17 cm and was measured in planar cross-bedded conglomerates (LFT Gp). In general, most LFTs possess moderate to poor sorting and, especially in the case of sandy and gravelly LFTs, indistinct bedding. Roundness, by contrast, is in the range of subrounded to well-rounded in the gravelly lithofacies (Fig. 5A), and subangular to subrounded in the sandy lithofacies. Neighbouring sand grains display various kinds of contacts ranging from floating grains to point-convex, long-convex and concave-convex-contacts (Fig. 5B). Under the microscope, many quartz grains exhibit corrosion, which is reflected by margins frayed on a micron-scale, and up to 100 μm large holes (Fig. 5C). The XPL images prove a prevalence of undulose extinction. Detrital quartz shows a short-lived blue CL of the 440 nm emission band (Fig. 5D), whose intensity varies across a single grain: whereas highly intense CL is restricted to a 20 to 40 μm thick zone along the outer margins of the grains and areas along fractures, low-intensity CL occupies internal areas (Fig. 5D). Intergranular space is almost completely sealed by dispersed hematite (Fig. 5B), up to 500 μm large corroded calcite crystals and clay minerals (Fig. 5C). The clays mainly consist of dickite (as proven by X-ray diffraction) occurring as stacked bundles of discoid crystals. Acicular illite and kaolinite-group minerals form negligible components. The illite mineral does not show any swelling with ethylene glycol. Detailed polytype analysis of the micaceous phase(s) was not possible owing to the low content in the clay separates, but significant line broadening of the basal reflections and the absence of 2M1 polytype reflections indicates the presence of rather disordered illite of possible diagenetic origin. Clay minerals also fill in fractures and holes left by corrosion within quartz grains and calcite crystals, supporting the hypothesis of formation in a late stage of diagenesis.

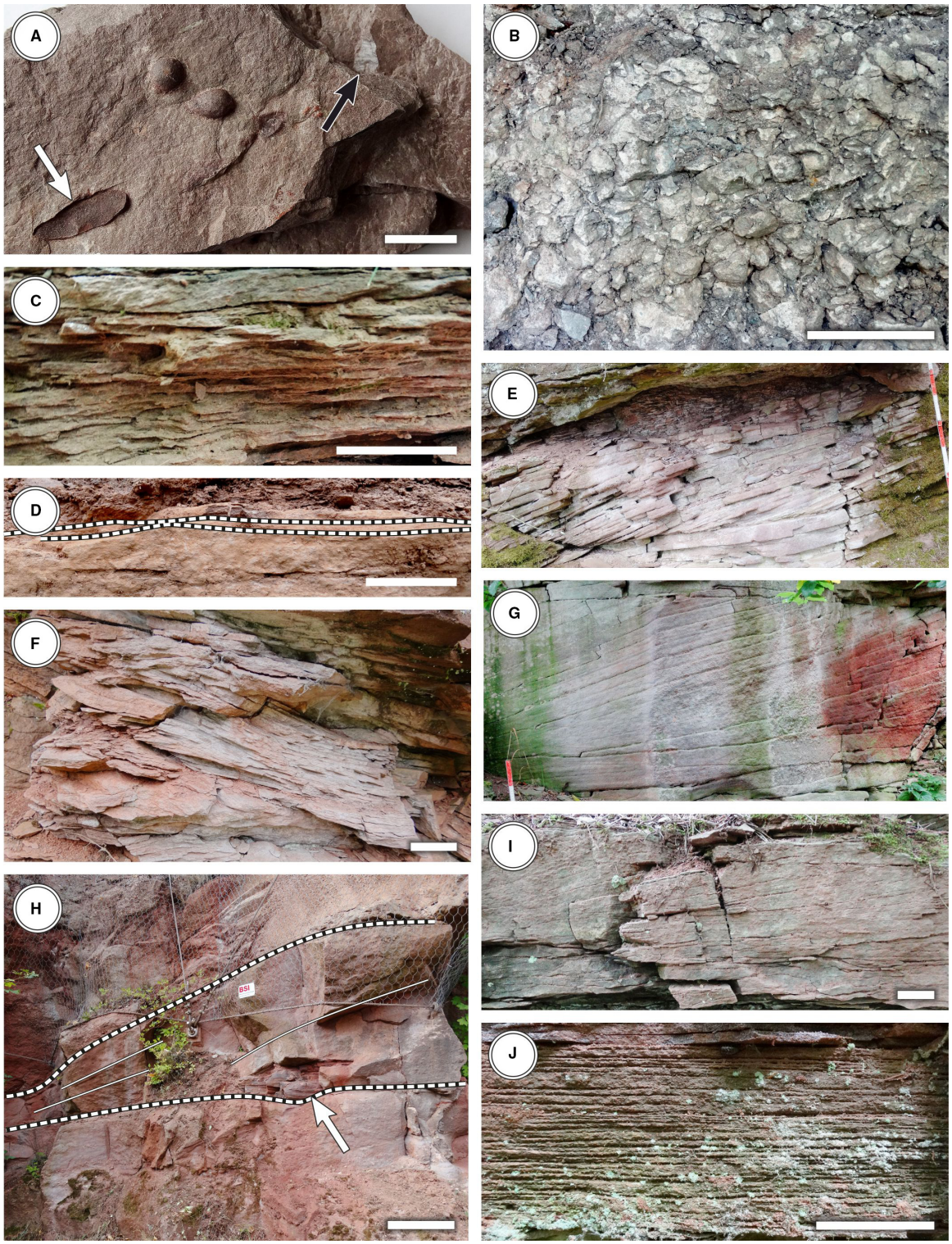

Fig. 3. Fine-clastic and sandy lithofacies types. Length of one red section on the rule: 10 cm. Length of white scale bar: 5 cm [50 cm in (H)]. (A) Vertisol (LFT Pv). Note siderite nodules (white arrow) and slickensides (black arrow). (B) Calcisol (LFT Pc). (C) Siltstones showing uneven horizontal bedding (LFT Fh) and ripple cross-bedding (LFT Sr). (D) LFT Sr showing wave-ripple bedding. (E) Planar cross-bedded sandstone (LFT Sp). (F) Small-scale trough cross-bedded sandstone (LFT St). (G) Medium-scale trough cross-bedded sandstone (LFT St). (H) Cross-bedding transitional from LFT Sp to LFT St as part of a downstream-accretion element overlying a petrified trunk (arrow). (I) Low-angle cross-bedded sandstone (LFT Sl). (J) Horizontally bedded sandstone (LFT Sh).

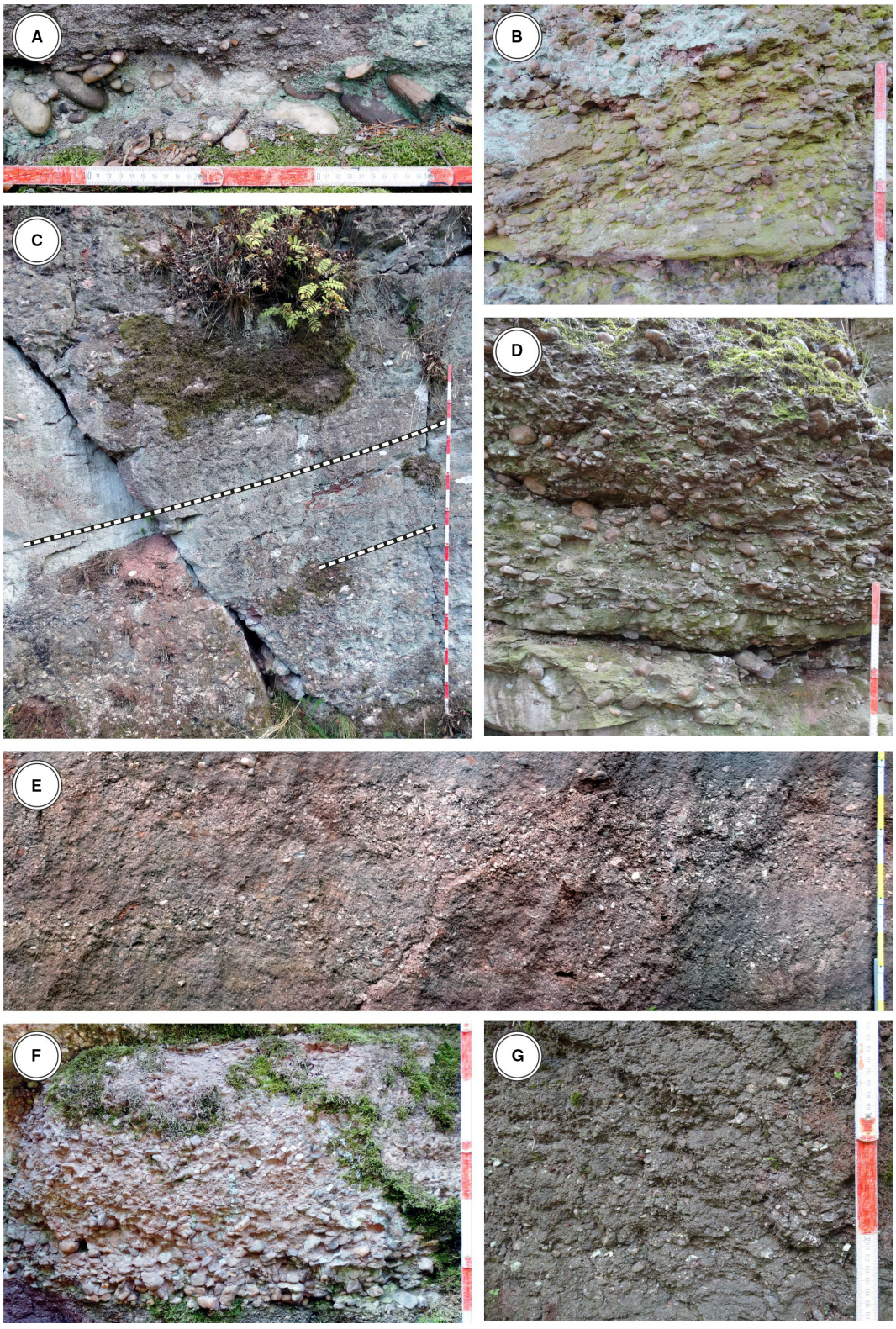

Fig. 4. Gravelly lithofacies types. Length of one red or yellow section on the rule: 10 cm. (A) Conglomerate showing imbrication (LFT Gim). (B) Planar-cross bedded conglomerate (LFT Gp). (C) Trough cross-bedded conglomerate (LFT Gt). (D) Conglomerate sheet showing horizontal stratification (LFT Gh). (E) Inversely graded conglomerate (LFT Gi). (F) Massive, clast-supported conglomerate (LFT Gcm). (G) Massive, matrix-supported conglomerate (LFT Gmm).

Table 2. Description and interpretation of lithofacies types (compiled and modified after Legros, 2002; Miall, 2006; Schneider *et al.*, 2010).

Facies code	Facies description (including figure reference)	Genetic process
Pv	Siltstone, pale greenish red, clayish, weakly horizontally stratified, frequent slickensides and up to 2 cm large ellipsoid to spherical siderite concretions (Fig. 3A)	Vertisol formed subaerially under alternating water contents
Pc	Siltstone, greyish red, clayish, non-stratified, abundant nodular calcareous concretions 1 to 2 cm in diameter (Fig. 3B)	Calcisol formed subaerially under seasonally dry conditions
Fb	Siltstone, red, fine sandy, bioturbated by *Scoyenia* ichnia (Fig. 6B)	Bioturbation of fine-clastics under alternating inundation
Fh	Siltstone, red, fine sandy, rarely clayish containing randomly alternating sets of indistinct horizontal bedding, and ripple cross-bedding on a 0·5 cm scale (Fig. 3C)	Very low-energetic subaquatic deposition alternating between unidirectional laminar flow and non-flowing conditions
Sr	Fine-grained sandstone, pale red, ripple cross-bedded, two subtypes with respect to symmetry: asymmetrical and symmetrical (Fig. 3D)	Current ripples and wave ripples
Sp	Fine-grained sandstone, pale red, planar cross-bedded (Fig. 3E)	2D dunes
St	Fine to coarse-grained sandstone, pale red to reddish grey, may be pebbly, through to cross-bedded, three subtypes with respect to bed thickness: small-scale (<20 cm, Fig. 3F); medium-scale (20 to 200 cm, Fig. 3G); and large-scale (>200 cm, Fig. 3H)	3D dunes
Sl	Fine-grained sandstone, pale red, low-angle cross-bedded (Fig. 3I)	Low-angle dunes
Sh	Fine to medium-grained sandstone, pale red, horizontally laminated at millimetre-scale (Fig. 3J)	Sand sheets (upper plane bed)
Gim	Fine to coarse-grained conglomerate, clast-supported, well-sorted matrix comprising medium-grained sand, imbricated bedding (ab plane imbrication) (Fig. 4A)	Imbricated channel lag due to transport of gravel as bedload
Gp	Conglomerate, poorly sorted, clast to matrix-supported, indistinctly planar cross-bedded (Fig. 4B)	Transverse bedforms
Gt	Conglomerate, poorly sorted, clast to matrix-supported, indistinctly trough cross-bedded (Fig. 4C)	Transverse bedforms or channel fills
Gh	Conglomerate, poorly sorted, clast to matrix-supported, indistinctly horizontally bedded (Fig. 4D)	Gravel sheet
Gi	Conglomerate, clast-supported, inverse-graded (Fig. 4E)	Clast-rich debris flow with inverse grading due to kinetic sieving
Gcm	Conglomerate, poorly sorted, clast-supported, massive to normal-graded (Fig. 4F)	Inertial bedload of hyperconcentrated flows
Gmm	Conglomerate, very poorly sorted, angular to subrounded pebbles up to 1 cm in diameter, matrix-supported (matrix in the range of silt to coarse sand), massive (Fig. 4G)	Plastic debris flow

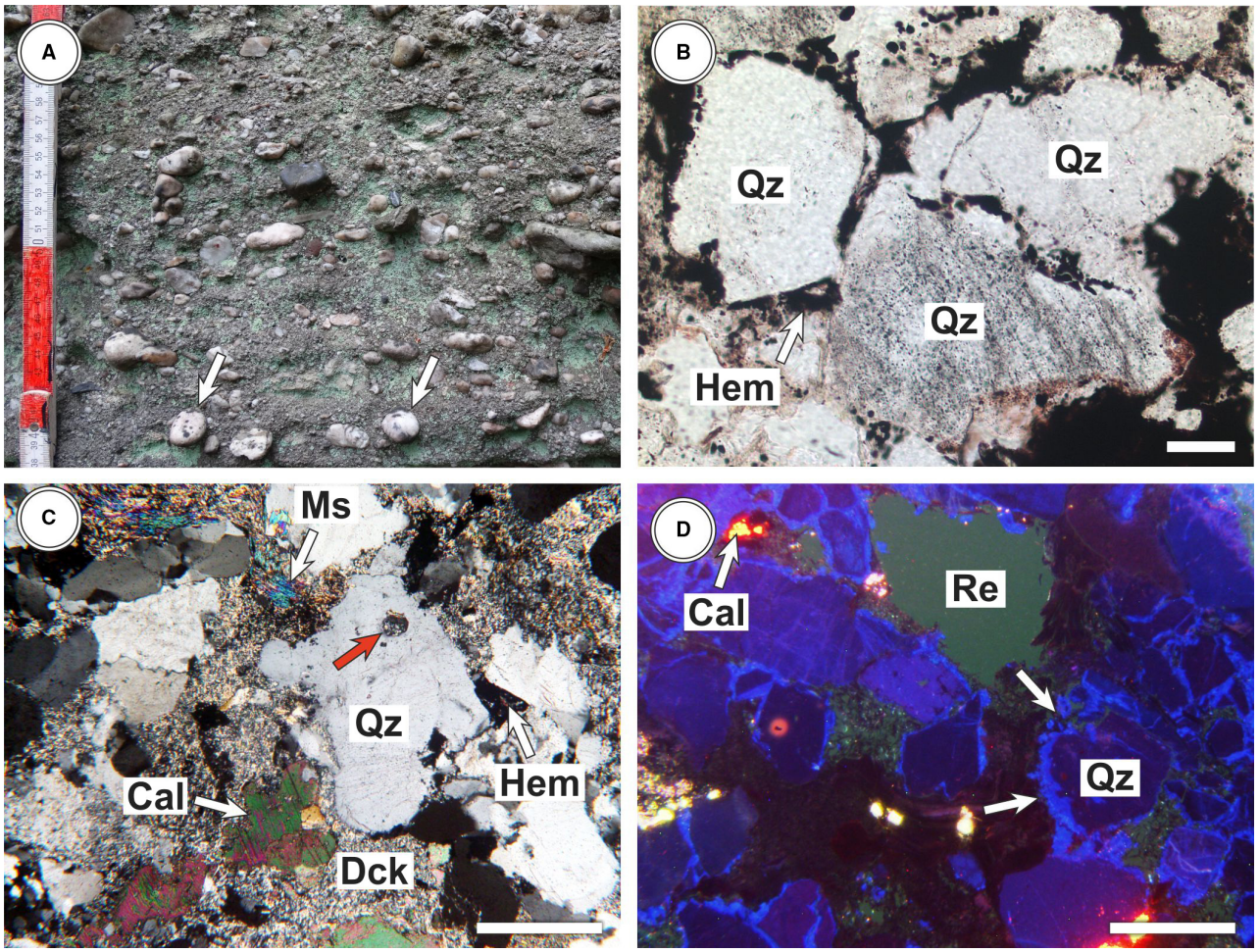

Fig. 5. Petrography of coarse-clastics. (A) Matrix-supported conglomerate containing subrounded and well-rounded (arrows) clasts. (B) Subangular quartz as the dominant component in the Kyffhäuser. Note hematite fringes around the grains; plane polarized light (PPL) image. (C) Composition of the Kyffhäuser coarse clastics: detrital quartz and muscovite, surrounded by a matrix consisting of calcite, dickite and hematite. Quartz grains are commonly perforated (red arrow). Cross-polarized light (XPL) image. (D) Cathodoluminescence (CL) image of a medium-grained sandstone. Quartz possesses a blue CL, whereas calcite exhibits a bright orange CL. Note increased CL intensity along the outer margins of the quartz grains (arrows). The resin, which filled empty intergranular spaces during processing, shows a greenish CL. Abbreviations: Cal: calcite; Dck: dickite; Hem: hematite; Ms: muscovite; Qz: quartz; Re: resin.

Lithofacies associations rarely providing woody debris

Six lithofacies associations ranging from fine-clastic-dominated to coarse-clastic-dominated are assigned to this group. Except for the channel-floodplain association, in which one 2 m long cast of a stem was found, fossil woody debris is extremely rare and restricted to silicified trunk fragments not exceeding 10 cm in diameter.

Floodplain association (Fig. 6A to C)

Description: Because of the dominantly fine-clastics, exposures of this LFA erode to gentle slopes, and they are usually concealed by muddy soils. Accordingly, the few outcrops are restricted to quarries and road cuts (Fig. 6A). The floodplain association mainly consists of fine sandy siltstone forming a vertical and random, centimetre-scale alternation of laterally extensive ripple cross-bedded to horizontally bedded fine-clastics (LFT Fh) and strongly bioturbated beds (*Scoyenia* ichnofacies, LFT Fb, Fig. 6B). Each of the beds extends across a few metres lateral distance. Intercalations of a few centimetres thick siltstone beds comprising up to 4 mm thick and 2 cm long root traces in low abundance (LFT Fro), and of up to 50 cm thick

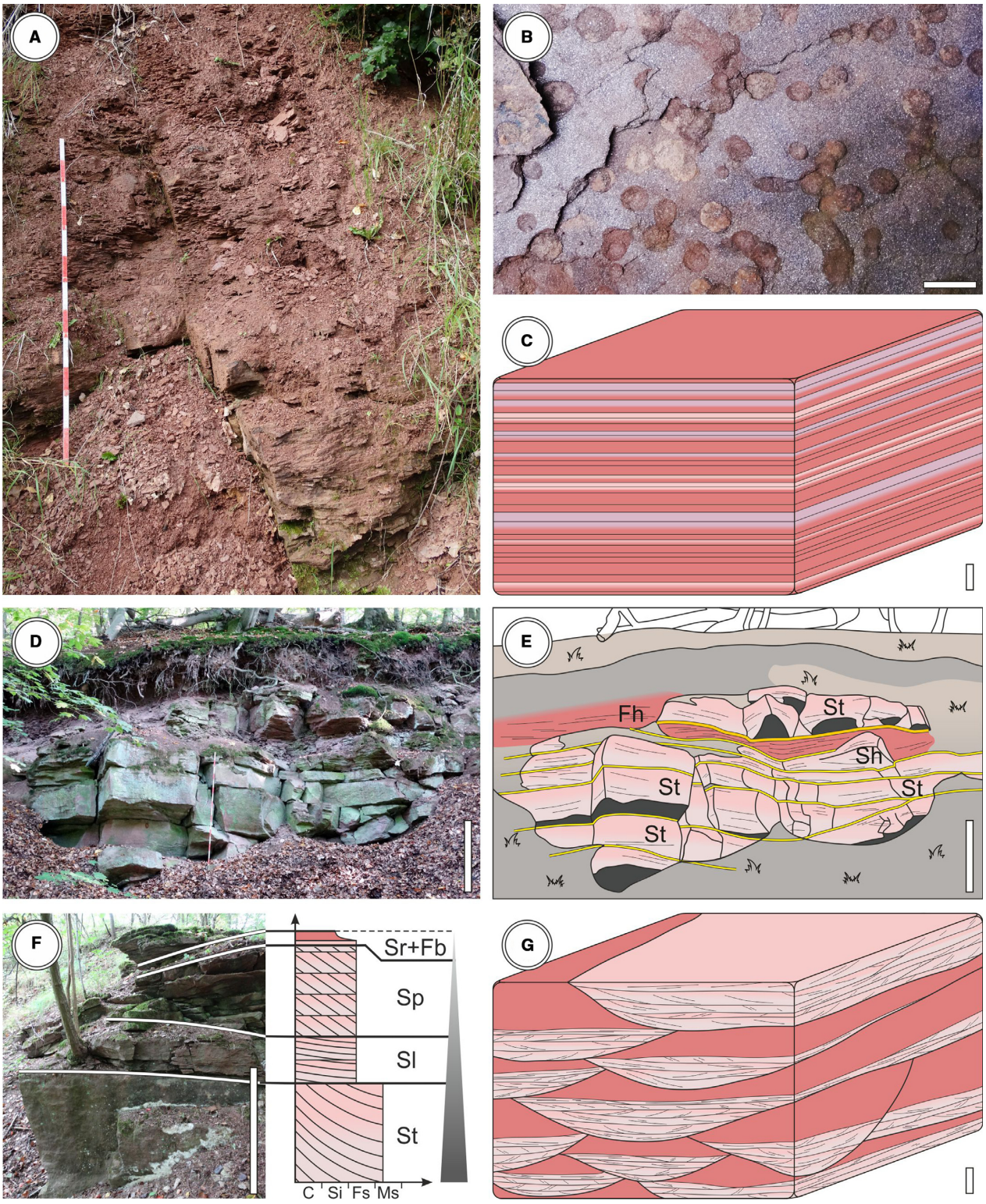

Fig. 6. Floodplain (A) to (C) and sandy channel (D) to (G) lithofacies associations (LFAs). White scale: 1 m; one red bar on the rule: 10 cm. (A) Floodplain LFA. Note upward-fining from fine sandy siltstones at the base to clayish siltstones at the top. Scale: 1 m. (B) *Scoyenia* trace fossils on a bedding plane (LFT Fb). Scale: 1 cm. (C) Simplified block model of the floodplain LFA. Scale: 1 m. (D) Stacked channels of the sandy channel association. Scale: 1 m. (E) Facies architecture derived from (E). Scale: 1 m. (F) Detail of a fining-upward cycle. Scale: 1 m. (G) Simplified block model of the sandy channel LFA. Scale: 1 m. For abbreviations see Table 2.

beds of immature Calcisols and Vertisols (LFTs Pc and Pv) occur rarely (Fig. 3A and B). The abundance of the three latter LFTs increases in a profile-up direction.

Interpretation: The single lithofacies recognized in this association reflects low-energy flow and standing water body deposition (LFT Fh) in a floodplain environment interrupted by phases of subaerial exposure leading to palaeosol formation (LFTs Pc and Pv), vegetation establishment (LFT Fro) and bioturbation (LFT Fb; Keighley & Pickerill, 2003; Schneider *et al.*, 2010). Density and size of the roots, together with palaeosol immaturity point to comparatively short subaerial phases and weakly developed sparse vegetation lacking large plants.

Sandy channel association (Fig. 6D to G)

Description: This LFA was the second most important target of sandstone quarrying in the Kyffhäuser owing to its abundant well-sorted sandstones suitable for manufacturing building blocks (Fig. 6D). In cross-sections perpendicular to the palaeocurrent direction, lenticular sandstone units range from 2 to 4 m in thickness and reach 15 m in width, and possess a concave-up erosional base (Fig. 6E). An internal upward-fining is present (Fig. 6D to F) starting with a sequence of up to five, less than 1 m thick beds of the LFTs St and Sh. Gravel forms a minor component or may be absent. This basal sequence is overlain by medium-scale to small-scale beds of the LFTs Sl and Sp (Fig. 6F). The topmost beds comprise small-scale ripple cross-bedded sandstones (LFT Sr) and siltstones containing *Scoyenia* trace fossils (LFT Fb). The topmost beds of fine-clastics are not preserved in all cases owing to post-depositional erosion.

Interpretation: Given their concave-up erosional base, their lenticular outline and internal fining-upward, the sandstone units are interpreted as channels (Miall, 1977, 2006). The vertical succession of LFTs within a channel recorded the progressive filling, which resulted from both decreasing water depth and stream velocity.

Channel-floodplain association (Fig. 7A to E)

Description: This LFA is limited in its exposure and found only in one quarry. The channel-floodplain association shows the strongest facies gradients in the Kyffhäuser both vertically and laterally (Fig. 7A, B and E). Floodplain elements comprise less than 0·5 m to almost 2·0 m thick beds of LFTs Pc and Fh. These beds can be truncated laterally (Fig. 7A and B), or are overlain erosively by <0·5 to 1·8 m thick channels consisting of LFT Sp or St. Furthermore, sandy LFTs show strong variations in grain size, sorting and composition ranging from moderately to well-sorted quartz sandstones to poorly sorted gravelly sandstones rich in reworked, probably pedogenic hematite glaebules (Fig. 7C and D). One horizontally aligned, highly compacted stem cast was documented reaching at least 2 m in length and 20 cm in width.

Interpretation: A floodplain environment dissected by fluvial channels is interpreted to represent this LFA. Sedimentation was dominated by low-energy unidirectional fluid flow (LFT Fh) interrupted by long-lasting phases of subaerial exposure and pedogenesis (LFT Pc). In fluvial channels, subcritical turbulent fluid flow deposited cross-bedded coarse clastics (LFTs Gt, St and Sp).

Gravel barform-channel association (Fig. 7F to I)

Description: This LFA is barely exposed, and can be mostly found in road cuts. It is made up of simple gravel barforms and channels. The first reach a thickness of 1·5 m, and consist either of upward-fining trough cross-bedded conglomerates (LFT Gt, Fig. 7F) or clast-supported massive conglomerates (LFT Gcm, Fig. 7G). Channel fills initiate with massive conglomerates (LFT Gcm) and are overlain by <50 cm thick sets of trough cross-bedded sandstones (LFT St). Rarely, up to 20 cm thick beds of well-sorted planar cross-bedded and trough cross-bedded sandstones occur. In comparison to the other LFAs, the gravel barform-channel association is rich in poorly sorted LFTs, and bedding, if present, is usually indistinct. Sandstones are always coarse-grained (Fig. 7H). The occurrence of LFT Gmm in the Kyffhäuser section is limited to the gravel barform-channel association (Fig. 7G).

Interpretation: Gravel barforms and channels of this LFA were deposited by highly energetic fluid flows to hyperconcentrated flows, as reflected by sorting, indistinct bedding and high proportions of clast-supported massive conglomerates. Trough cross-bedded conglomerates (LFT Gt) showing upward-fining represent humpback bars, whose formation was connected to gravel overpassing and a bimodal gravel-sand supply (Allen, 1983). Rare intercalations of LFT Gmm indicate low frequency flow deposition.

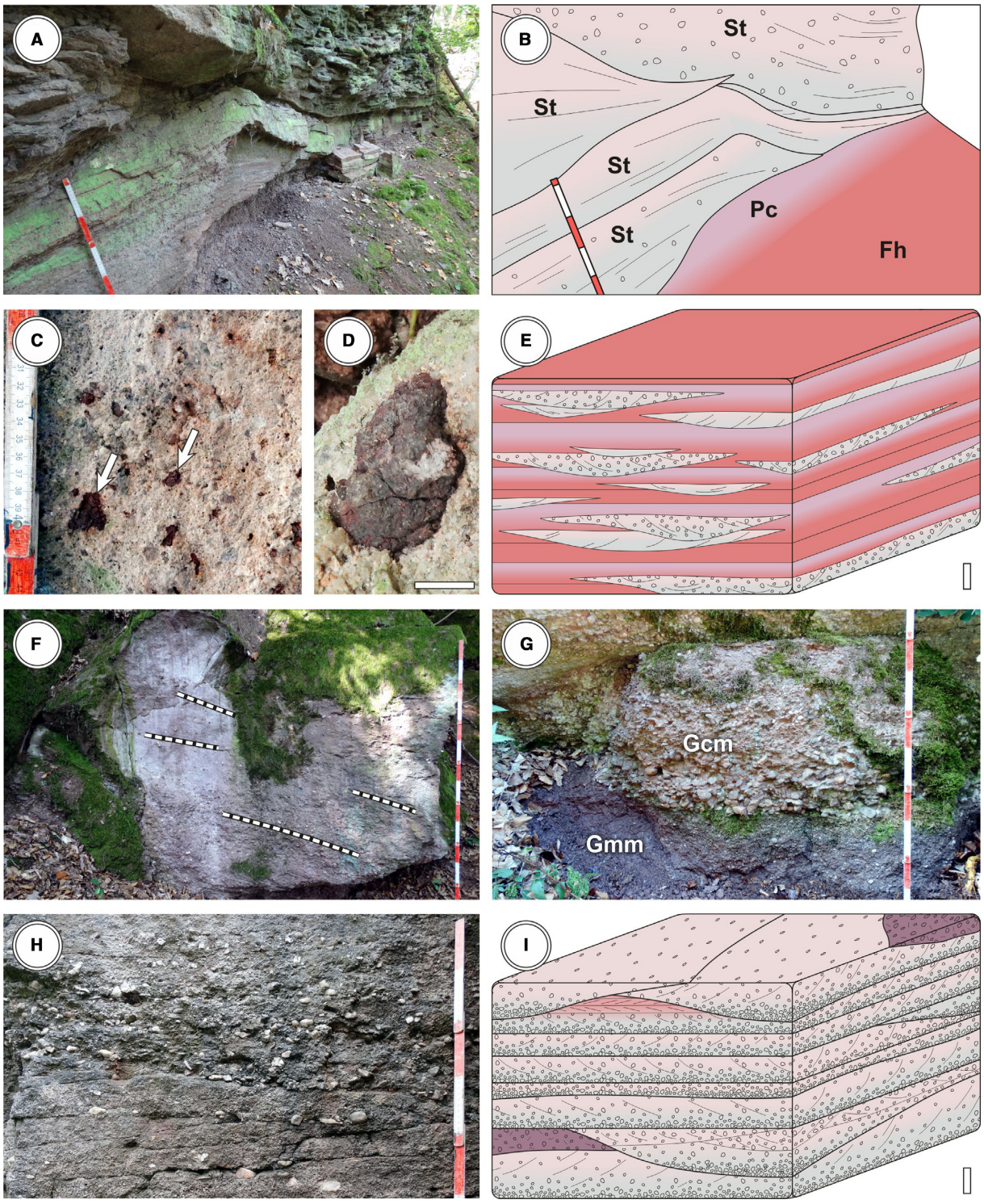

Fig. 7. Channel-floodplain (A) to (E) and gravel barform-channel (F) to (I) lithofacies associations (LFAs). White scale: 1 m; one red bar on the rule: 10 cm. (A) Quarry west of the village Ichstedt (eastern Kyffhäuser) showing strong vertical and lateral facies gradients. (B) Facies architecture derived from (E). (C) Trough cross-bedded gravelly sandstone (LFT St) containing abundant hematite clasts (arrows). (D) Detail of a hematite clast. Scale: 1 cm. (E) Simplified block model of the channel-floodplain LFA. (F) Trough cross-bedded conglomerate (LFT Gt) showing normal grading and cross-beds (lines). (G) Matrix-supported massive conglomerate (LFT Gmm) erosively overlain by clast-supported massive conglomerate (LFT Gcm). (H) A succession of pebbly trough cross-bedded sandstones (LFT St). (I) Simplified block model of the gravel barform-channel association.

Simple-gravel barform association (Fig. 8A to C)
Description: This lithofacies association forms steep slopes and hills, and is exposed in road cuts, cliffs and quarries (Fig. 8A). The tabular structure is based on decametres-thick successions of 1·5 to 2·5 m thick and several decametres to less than 100 m wide conglomerate sheets (LFT Gh), trough cross-bedded and massive conglomerate beds (LFTs Gt and Gcm, Fig. 8A and C). Intercalations of LFT St occur rarely. Bounding surfaces separating conglomerate beds and conglomerate sheets may be accompanied by a few centimetres thick gravel lags or <25 cm thick intercalations of LFT Fh (Fig. 8B). Usually, the latter pinch out laterally across a 1 m distance.

Interpretation: Gravel barforms. Based on grain sizes, sorting, tabular geometry and composition, the conglomerate sheets and beds point to deposition by traction currents, hyperconcentrated and mass flows. Whereas these coarse-clastics represent flooding events, intercalations of gravel lags and erosional remnants of fine-clastics (LFT Fh) point to phases of reduced discharge and stream velocity (Ferguson & Werritty, 1983; Wooldridge & Hickin, 2005; Miall, 2006). Such deposits especially form during the waning flood when stream velocity is no longer sufficient to transport gravels or even to erode them, resulting in the formation of thin fine-grained sediment sheets on barforms (Wooldridge & Hickin, 2005). Later floods may erode these bar-top sediments partially or even completely.

Complex-gravel barform association (Fig. 8D to G)
Description: Outcrop areas of this LFA are characterized by steep slopes and cliffs (Fig. 8D). In vertical two-dimensional sections, the complex-gravel barform association forms up to 2 m thick tabular units, which extend laterally across decametre distances (Fig. 8D to G). Both the base and the top are flat and erosional (Fig. 8D and E). Internally, these units consist of a vertical succession of 15 to 50 cm thick tabular beds of conglomerate sheets (LFT Gh), planar cross-bedded conglomerates (LFT Gp) and imbricated conglomerates (LFT Gim, Fig. 4A). However, bounding surfaces separating conglomerate beds may be accompanied by less than 30 cm thick sandstone intercalations (LFTs Sp and St), which usually pinch out laterally across distances of several decimetres or even metres (Fig. 8E). If occurring, these sandstone intercalations show a sharp, irregular base reflecting the erosion of the underlying conglomerate. The complex-gravel barform association hosts the largest clast diameters in the Kyffhäuser of up to 17 cm, and commonly yields well-rounded pebbles (Fig. 8F).

Interpretation: Based on their complex structure, gravel barforms of this association were deposited by repeated flooding events. Whereas tabular conglomerate beds result from high-discharge stages, erosional bounding surfaces and associated sandy bedforms indicate processes operating under falling discharge (Miall, 2006). In contrast to the simple-gravel barform association, the higher proportion of sandy bedforms, cross-bedded conglomerates and imbricated conglomerates in the complex-gravel barform association reflects a higher abundance of water flow deposition.

Lithofacies associations containing abundant large woody debris

As opposed to the previous lithofacies associations, sediments of the sandy bedform and multiple-element associations provide common petrified trunks usually embedded horizontally and occurring in isolation.

Sandy bedform association (Fig. 9A to D)
Description: This LFA is the best-exposed in the Kyffhäuser and its sandstones were the main objective for sandstone quarrying in the region for centuries. Lithofacies architecture is based on stacked sandy bedforms possessing a lenticular outline in vertical sections. Bedform thickness is 0·5 to 2·0 m, whereas its width ranges from 10 m to several decametres (Fig. 9A to C). Both the base and the top are erosional and can be accompanied by petrified trunks being several metres in length (Fig. 9C). Internally, each bedform is composed of either a single LFT St (Fig. 9B), or a complex arrangement of small-scale beds of St, Sp, Sl and Sh. In the latter case, weak normal grading may be present, starting with gravelly medium to coarse-grained sandstones at the base, and fine to medium-grained sandstones at the top. Rarely, intercalations of up to 4 m thick sandstone channels and medium-scale trough cross-bedded conglomerates (LFT Gt) are represented.

Interpretation: Stacked lenses of trough cross-bedded sandstones are interpreted as channel-floor dune fields (Miall, 2006) considered to be one depositional setting for the sandy bedform association. In addition, sandy bedforms showing normal grading and a complex internal structure of small-scale bedforms may represent sand bars. During sedimentation, variable discharge resulted

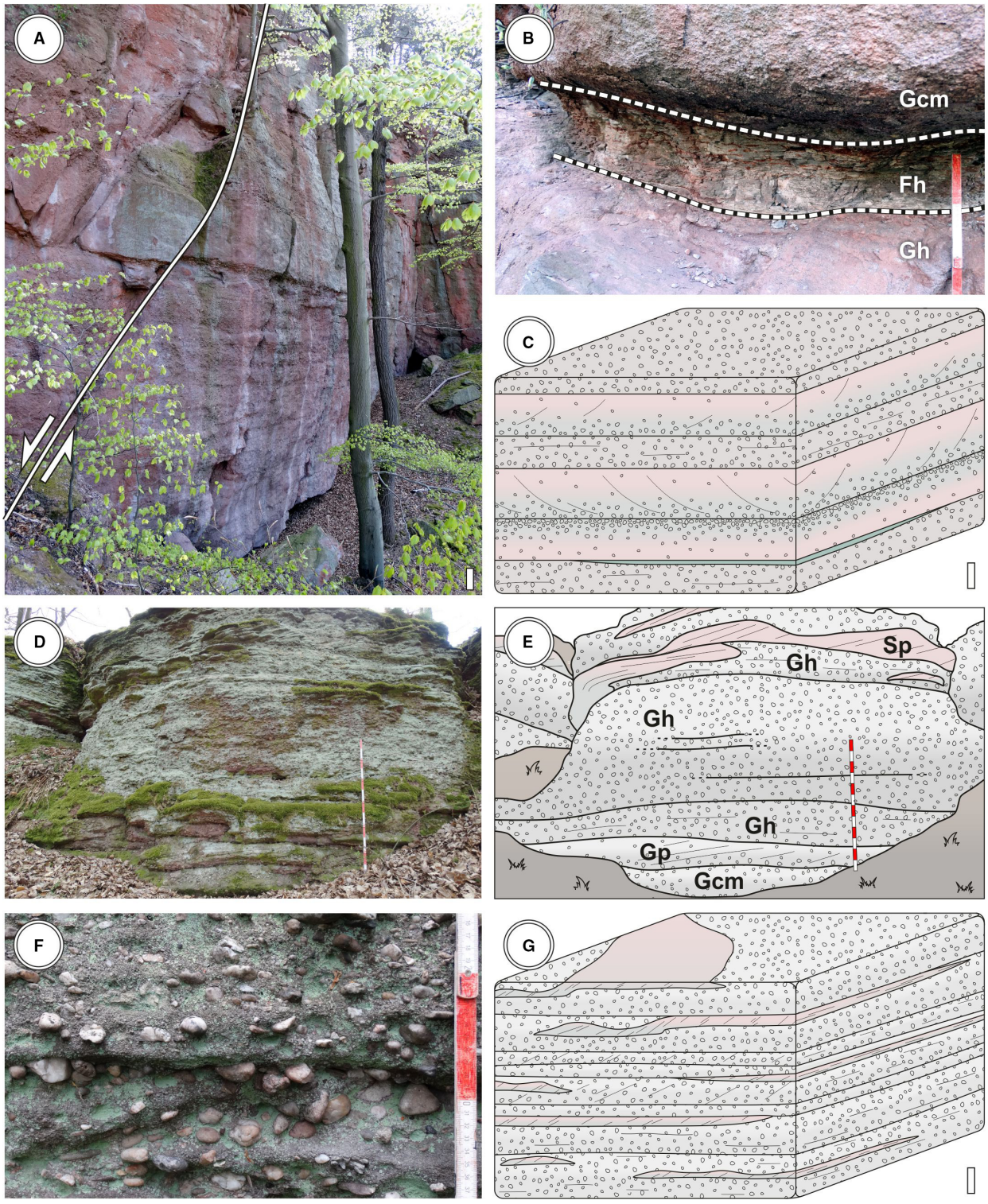

Fig. 8. Simple-gravel barform (A) to (C) and complex-gravel barform (D) to (G) lithofacies associations (LFAs). White scale: 1 m; one red bar on the rule: 10 cm. (A) Conglomerate bed succession of the simple-gravel barform association. (B) Bar-top siltstones (LFT Fh) underlain and overlain by conglomerate beds reflect the waning flood stage. (C) Simplified block model of the simple-gravel barform LFA. (D) A succession of medium-scale conglomerate beds with intercalated sandy bedforms. (E) Facies architecture derived from (D). (F) Detail of a horizontally bedded conglomerate (Gh) showing well-rounded clasts. (G) Simplified block model of the complex-gravel barform LFA.

in the deposition of bedforms pointing to subcritical flow (LFTs Sp, St, Sl and Sh). Moreover, the waning flow is represented by erosional surfaces containing large woody debris (Tyler & Ethridge, 1983; Miall, 2006).

Multiple-element association (Fig. 9E to H)
Description: This LFA is highly variable with respect to its architectural element composition both vertically and laterally (Fig. 9E and F), and contains gravel barforms, sandy bedforms, downstream-accretion elements and channels. The <2 m thick gravel barforms and conglomerate sheets exhibit a simple structure, and consist either of the LFTs Gi, Gh or Gt. Sandy bedforms and downstream-accretion elements are composed of LFT St. Channels ranging from a couple of decimetres to 4 m in thickness have an upward-fining fill starting with massive conglomerates (LFT Gcm), followed by cross-bedded sandstones (LFTs St, Sp and Sr, Fig. 9G). Channels may lack gravelly LFTs and, thus, start with trough cross-bedded sandstones (LFT St; Fig. 9F). Depending on the predominant architectural element, transitions to other LFAs are possible.

Petrified stems up to several metres in length are embedded horizontally and in isolation, and their stratigraphic occurrence is limited to sedimentary bounding surfaces, i.e. the top/base interfaces in a vertical sequence of architectural elements (Fig. 10). Four cases were documented: (i) a stem is both underlain and overlain by a sandy bedform; (ii) a stem is both underlain and overlain by a gravel barform; and (iii) a stem is underlain by a gravel barform but overlain by a sandy bedform; or (iv) vice versa.

Interpretation: This LFA recorded high-discharge events represented by gravel barforms, conglomerate sheets and downstream-accretion elements. Barform disruption during floods generated grain flows showing inverse grading resulting from kinetic sieving (LFT Gi; Nemec *et al.*, 1980; Legros, 2002). The falling-flow and low-flow stages are represented by fossil LWD which stranded on barforms during the waning flood (Alexander *et al.*, 1999). The high variability of architectural elements reflects frequent and considerable changes in depositional conditions, i.e. stream velocity, sediment content and water depth.

Large woody debris-induced sedimentary structures (LWDISS)

Fossil trunks from the sandy bedform and multiple-element associations are accompanied by a variety of sedimentary structures being formed during stranding and entombment of large woody debris. By analogy to microbially induced sedimentary structures ('MISS') according to Noffke *et al.* (2001) and vegetation-induced sedimentary structures ('VISS') as defined by Rygel *et al.* (2004), sedimentary structures caused by the interaction of large woody debris and detrital sediments are referred to as large woody debris-induced sedimentary structures ('LWDISS') herein.

Lateral deflection scours and lags
Description: Lateral deflection scours appear as erosion surfaces laterally bounding drifted trunks. In vertical sections, they are recognized as parabolic, concave-up, low-amplitude bounding surfaces starting at the specimen, and extending across a lateral distance of less than 2 m (Fig. 11A and B). If a drifted log was embedded in isolation and sub-parallel to palaeoflow, lateral deflection scours would be present symmetrically on both sides. However, in well-sorted deposits (for example, the sandy bedform LFA), lateral deflection scours may be easily overlooked owing to the lack of grain-size differences (Fig. 11A). In moderate to poorly sorted sediments, by contrast, erosional surfaces are accompanied by overlying gravel lags (Fig. 11D). Depending on mean grain size and stratification of the embedding sediment, these lags range from a few centimetres thick beds in stratified sandstones up to 30 cm thick and 50 cm wide mounds of clast-supported conglomerates in massive to poorly stratified conglomerates. Laterally deflected scour and lag surfaces extend from the specimen parallel to palaeoflow in the downstream direction.

Interpretation: Lateral deflection scours represent areas of increased stream velocity leading to erosion and lag formation. These areas were formed at the upstream termination of an obstacle (for example, woody debris), where the flow was split up into two helical eddies ('horseshoe vortices') bypassing the obstacle laterally (Baker, 1979; Abbe & Montgomery, 1996). The higher the stream velocity is during deposition, the coarser-grained and thicker the lateral deflection lags will be.

Underflow scour and fill
Description: Underflow scour and fills are found beneath logs, where they exhibit a bowl-shaped outline in vertical sections (Fig. 11B). Whereas the lower, concave-up boundary is erosionally

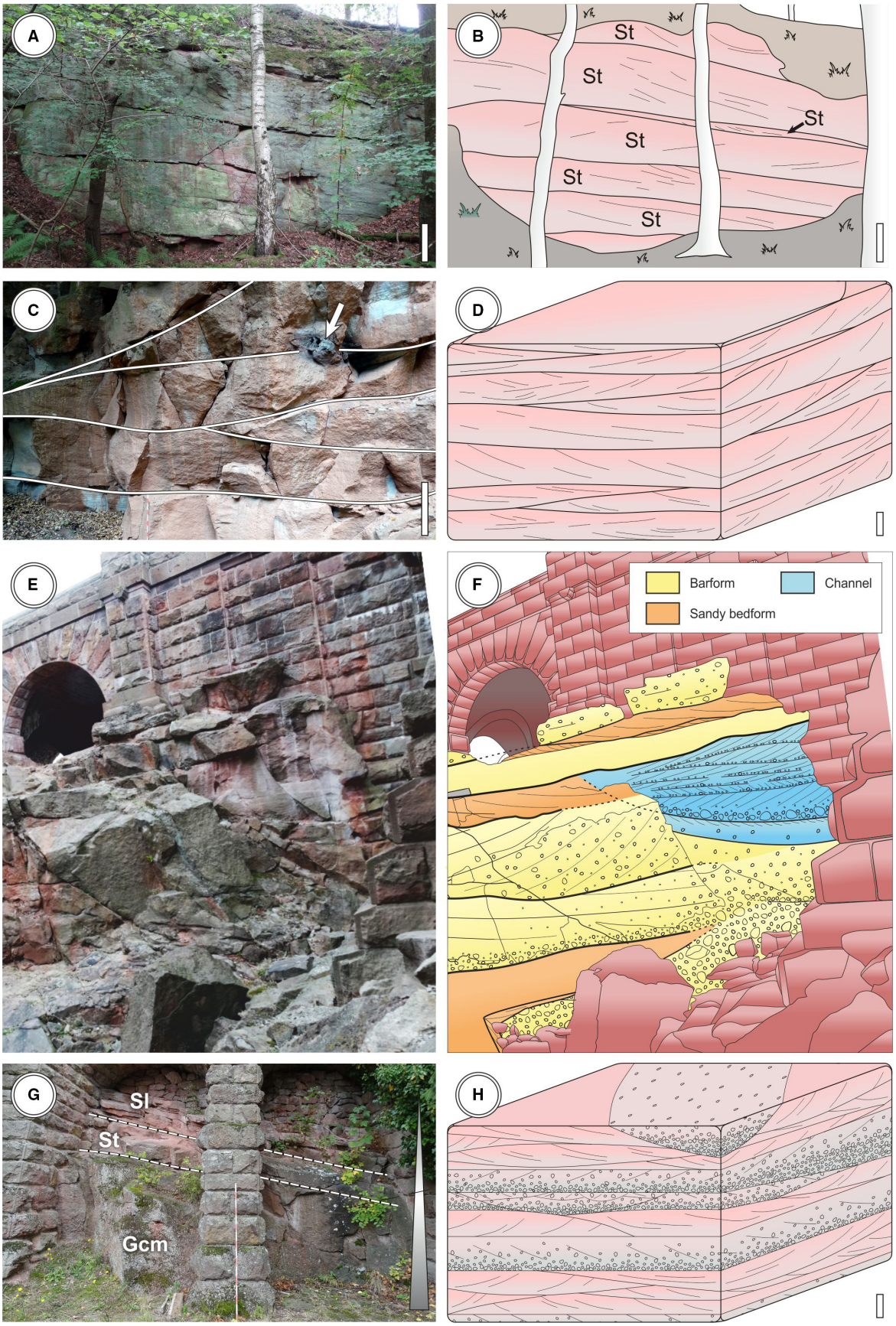

Fig. 9. Sandy bedform (A) to (D) and multiple element (E) to (H) lithofacies associations (LFAs). White scale: 1 m; one red bar on the rule: 10 cm. (A) Quarry north-east of Udersleben showing stacked sandy bedforms of well-sorted sandstones. (B) Facies architecture derived from (A). (C) Quarry north-west of Bad Frankenhausen. Note lateral outpinching and lenticular geometry of sandy bedforms (lines). Bounding surfaces may be accompanied by silicified logs (arrow). (D) Simplified block model of the sandy bedform LFA. (E) Outcrops of the multiple-element LFA at the Kyffhäuser Monument. (F) Lithofacies architecture in (A). (G) Upward-fining in channel deposits. (H) Simplified block model of the multiple-element LFA.

incised into the underlying strata, the upper boundary is predetermined by the overlying trunk. Internally, underflow scour and fills display three types of sediment fill: (i) clast-supported, massive gravel (LFT Gcm); (ii) a vertical succession of symmetrical beds consisting of gravel and sand (Fig. 11B); and (iii) an asymmetrical fill of trough cross-bedded gravelly sandstones (Fig. 11B).

Interpretation: Scouring beneath obstacles is connected to underflow and, thus, indicates free space or, at least, a negligible obstacle–sediment contact (Wallerstein *et al.*, 2001; Graf & Altinakar, 2017). Concerning LWD, such a case is provided if irregularly formed woody stems just selectively touch the sediment surface. Additionally, trunks can partially rest clear of the sediment surface if one termination is uplifted by still attached appendices (branches and roots) being stuck in the ground.

Sediment shadow bars

Description: These structures (defined by Joeckel *et al.*, 2015, and corresponding to channel-train ridges of Tooth & Nanson, 2000) are found downstream of trunks, which are embedded parallel to palaeoflow with their rootstock pointing in an upstream direction (Fig. 11A to C). If exposed in vertical sections perpendicular to palaeoflow (Fig. 11B), sediment shadow bars appear as symmetrical mound-like structures having a flat base and a convex-up top. The maximum thickness is achieved beneath the trunk (Fig. 11B). Internally, a stacking of form-concordant beds is found. Because of their shape and internal structure, sediment shadow bars prove to be aggrading rather than prograding laterally. The contact to the overlying trunk is characterized by underflow scouring (Fig. 11B).

Interpretation: Sediment shadow bar formation is attributed to reduced stream velocities on the leeward side of obstacles (rootstocks and crowns), where sediment accumulates beneath the attached trunk (Abbe & Montgomery, 1996; Fig. 11C). The lateral extent of sediment shadow bars is constrained by the width of the rootstock (Joeckel *et al.*, 2015).

Prod structures

Description: This structure is documented in a siltstone–sandstone succession underlying a rootstock whose trunk is pointing upstream (Fig. 11E to H). Whereas the rootstock is inserted into the underlying sandstone down to a depth of 30 cm, the attached stem base lies about 25 cm above the sandstone top (Fig. 11E and F). With respect to the underlying sandstone, beds gradually switch their dip direction towards the rootstock and finally plunge under the latter. This process is accompanied by decreasing bed thicknesses with minima to be reached beneath the petrified trunk (Fig. 11F). Because these observations are made from all exposed sides, a bowl-like three-dimensional geometry of the prod structure mirroring rootstock morphology is inferred. Beneath the rootstock, i.e. within the underlying sandstone, even small-scale variations in trunk morphology are repeated by stratification (Fig. 11F) proving soft-sediment deformation.

However, deformation structures related to the prod structure reach into greater depths. The undisturbed sedimentary succession beneath the trunk consists of a gravel barform, overlain by bartop siltstone and sandstone, upon which the fossil rootstock rests (Fig. 11G). Directly beneath the rootstock, this succession is highly disturbed. Owing to its bowl-like geometry, the sandstone prod structure has a concave-up base, which breaks through the underlying bar-top siltstone and touches the top of the conglomerate barform (Fig. 11G). Along with the sandstone/bar-top siltstone interface, centimetre-scale fluidization is present in the siltstone (Fig. 11H). In addition, the sandstone/conglomerate barform interface is a steeply inclining surface (dip angle: *ca* 45°) with a dip direction parallel to the transport direction of the rootstock.

Interpretation: The described characteristics are interpreted as relating to a prod mark caused

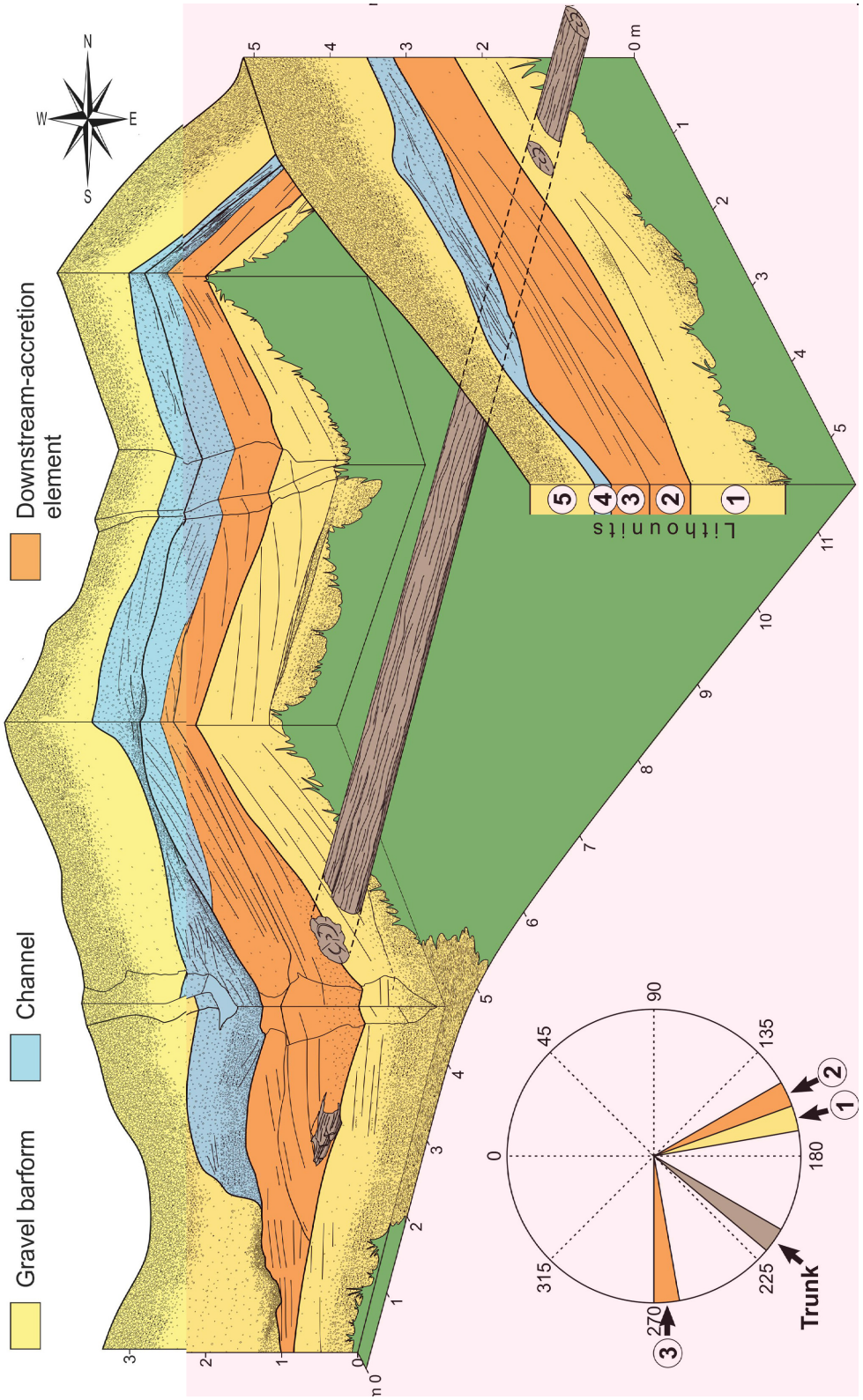

Fig. 10. Relation of drifted trunks and lithofacies architecture based on the multiple-element lithofacies association from the Burghof quarry, central Kyffhäuser (unit e, 51°24′46.39′′N, 11° 6′23.79′′E). Note the trunk's orientation subparallel to palaeoflow. Because the northern termination of the trunk penetrates the underlying gravel barform, both the deposition of the gravel barform (1) and grounding of the trunk resulted from a single flood event. Later, the trunk was buried by a downstream accretion element (2+3). This succession is overlain by channels (4) and another gravel barform (5).

by the impact of the rootstock on a barform (Fig. 11G). An oblique striking onto the sediment surface is inferred from the following characteristics: (i) the upstream towering stem base; and (ii) penetration of pre-existing sediments beneath the rootstock and their displacement in a downstream direction. Comprehensive plastic deformation of the sediments points to a high strain rate and, thus, reflect a large momentum of the impactor. This is additionally supported by the size of the rootstock. Local impact-related compression of pre-existing sediments was accompanied by plastic downward displacement of strata and lateral extrusion causing fluidization in fine-clastics (Fig. 11G and H). By the presence of extensive deformation structures in the sediments underlying fossil trunks, prod structures can be distinguished from underflow scour and fills.

Sedimentary environment and controlling processes

In general, the abundance and characteristics of gravelly and sandy lithofacies types (Figs 3, 4 and 12) and corresponding coarse-clastic lithofacies associations attest to a continental sedimentary setting characterized by aquatic, bedload-dominated, unidirectional deposition. Such a sedimentary style complies with fluvial systems but is also realized in alluvial/fluvial fans.

The alluvial fan model, however, cannot be supported based on various lithological evidence. First, well to moderately sorted, stratified sandstones and stratified to normally graded conglomerates (Figs 3 and 4), and their high proportion in the lithofacies associations, point to water flows and hyperconcentrated flows as the main depositional modes. Mass flow and sheet flood deposits – both being typical for deposition on fans (Blair & McPherson, 1994; Moscariello *et al.*, 2002) – occur rarely in the Kyffhäuser section and, if present, form part of gravel barforms. Second, floodplain deposits throughout the section (Figs 6A to C and 12) indicate fluvial systems or fluvial fans rather than alluvial fans (Nakayama & Ulak, 1999; Bashforth *et al.*, 2010). In addition, lithofacies analysis of the Kyffhäuser revealed architectural elements being indicative for a fluvial origin, including downstream accretion elements, gravel barforms and channels (Miall, 2006; Stikes, 2007). Bar-top fine-clastics (Fig. 8B), sedimentary bounding surfaces accompanied by large woody debris and related sedimentary structures (Figs 9C, 10 and 11) point to low-discharge stages, whereas gravel barforms, channel-floor dune fields and downstream-accretion elements prove episodic deposition under flood stage. This discharge ephemerality together with Calcisols, Vertisols and the occurrence of *Scoyenia*-type ichnia in the red floodplain deposits (wet red beds, *sensu* Schneider *et al.*, 2010) point to a tropical seasonal climate in the study area at the time of sedimentation. Finally, exhaustive palaeocurrent analyses carried out by previous workers, together with data collected in this study indicate a flow expansion angle well below 180° for all units of the Kyffhäuser section. Hence, an interpretation of the sediments as being formed in a dispersive alluvial or fluvial fan system is not supported by lithofacies leaving braided rivers as the environment of deposition.

The stratigraphic occurrence of lithofacies associations in the Kyffhäuser section (Fig. 12C) is regarded to reflect both spatial gradients and temporal changes in deposition. In a profile-up direction, two fining-upward cycles are evident, each representing a phase in the evolution of the sedimentary setting.

Phase 1: Basement burial (unit a to middle unit c)

Sediments of this phase possess strong lateral gradients in lithology based on three lithofacies belts formed by the gravel barform-channel, the simple-gravel barform and the sandy bedform LFAs (Fig. 12C). Because these lithofacies belts envelop the Kyffhäuser Crystalline Complex laterally and vertically, the basement is interpreted as an exposed part of a buried palaeoelevation (Fig. 13A). This model is additionally supported by palaeocurrent data: in units a and b, sediments were transported to the south-east and, thus, bypassed the basement. Starting with units $ß_2$ and c, which are the first units to extend across the basement, sediment transport changed to northern/north-eastern directions indicating that sedimentation has overtopped the basement barrier. Assuming that the top of floodplain unit $ß_2$ represents a quasi-horizontal surface (Fig. 12B and C), a rough estimation of the height of the palaeoelevation can be approximated from measuring the thickness of the (exposed) Siebigerode Formation below $ß_2$. Accordingly, a height of 100 m is obtained, being measured from the exposed stratigraphically lowest level of the Siebigerode Formation at profile EF relative to profile GH, where unit $ß_2$ overtops the basement (Fig. 12B). Based on the approximate palaeoelevation of 100 m and a

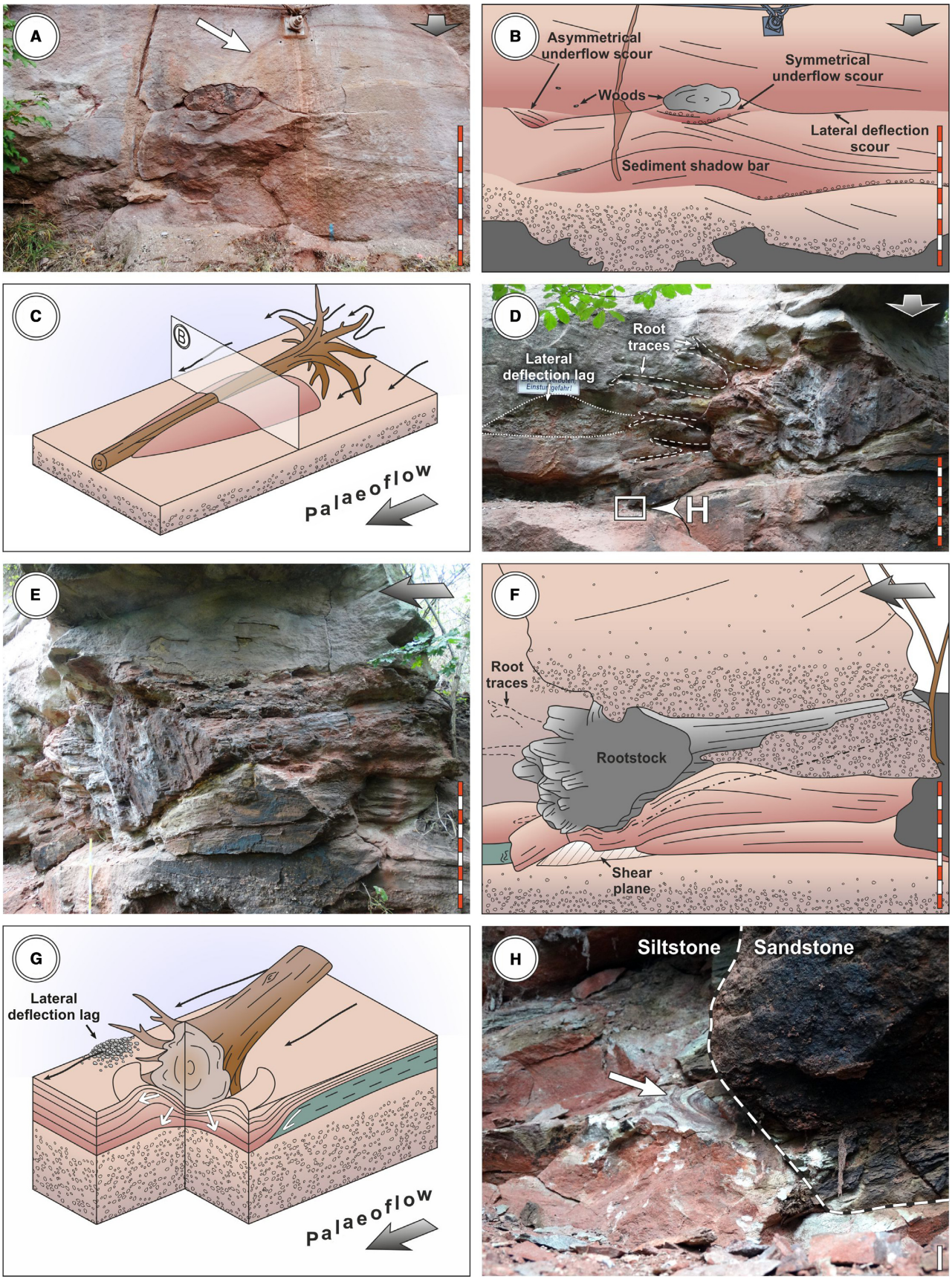

Fig. 11. Large woody debris (LWD) induced sedimentary structures. Grey arrows indicate palaeoflow. (A) Horizontally embedded trunk in downstream accretion element sandstones of the multiple-element lithofacies association (LFA). Note haloes of enhanced hematite cementation around the trunk (arrow). (B) Simplified sketch of (A) showing a complex combination of a sediment shadow bar, underflow scour and fills and lateral deflection lags reflecting the gradual burial of a trunk. (C) A genetic model of sediment shadow bars. (D) Lateral deflection lag of a rootstock. (E) Rootstock embedded in gravel barforms of the multiple-element LFA. (F) Simplified sketch of (E). Note uplifted upstream termination of the trunk. (G) A genetic model for prod structures connected to rootstock impact. (H) Detail of (D) exhibiting the contact of sandstone, which intruded into a bar top siltstone due to the impact of a rootstock. Note contorted lamination due to sediment fluidization (arrow). Scale: 1 cm.

lateral distance between the profiles EF and GH of 1500 m (Fig. 12C), a minimum basement gradient of 4° or 7% is calculated. Original palaeoelevation height and slope gradients may have been higher or lower depending on the impacts of syndepositional erosion as well as syn-depositional and post-depositional tectonics.

Lithofacies belts of units a+b hence prove the differentiation of the fluvial system into a main braid (gravel barform-channel and simple-gravel barform LFAs) proximal to the palaeoelevation, and a distal side braid (sandy bedform LFA; Fig. 13A). The term 'braid' is preferred here instead of 'channel' because there is no single channel in a braided river system, and also in order to avoid confusion with the architectural element 'channel'. 'Braid' hence refers to an area of diverging, intersecting and merging channels separated by barforms. However, inferred from the simple-gravel barform LFA, the main braid achieved widths of several 100 m and water depths of a couple of metres during floods. Close to the basement, poorly established stratification and sorting together with rare intercalations of mass flows in the gravel barform-channel LFA (Fig. 7G) were probably connected to alluvial inflows derived from the basement elevation, which increased sediment load locally (Fig. 13A). Lateral or spatial facies differentiation is known from modern braided-river systems in valleys, such as the Murchison River, New Zealand, the South Saskatchewan River, Alberta/Canada and the South Canadian River, Texas/USA (Miall, 1977). Lithological differentiation is connected to different topographic levels resulting from temporal downcutting (Miall, 1977).

In the middle unit c (Fig. 12C), the sandy bedform association gains increasing importance and dominates fluvial lithofacies across the Kyffhäuser. This change infers sand-bed braided rivers reflecting lowered stream competency and slope gradients possibly connected to basement burial (Fig. 12B).

Phase 2: Tectonic perturbation and reorganization (upper unit c to unit k)

This phase begins with a sudden increase in grain size and lithofacies gradients recorded by the multiple-element and complex-gravel barform associations in the upper unit c and unit e (Fig. 12C). These lithological changes mirror enhanced fluvial competency and indicate a strengthened relief as reconstructed for early phase 1; but, in contrast to the latter, maximum thickness during phase 2 has been achieved further east (Fig. 12C) indicating a syndepositional displacement of the subsidence centre (Fig. 12C). Accordingly, and because sediments do not provide any evidence for increasing or decreasing ephemerality because it would result from increasing or decreasing aridity, synsedimentary tectonics most likely initiated the onset of phase 2. In the Kyffhäuser Crystalline Complex, tectonic movements are also recorded by variously orientated normal faults, which were dated by Franzke *et al.* (2007) as being coeval to deposition of the overlying Stephanian strata based on co-genetic quartz–hematite mineralization. According to Schneider *et al.* (2005), the occurrence of differential tectonics in the Saale Basin was connected to north-west/south-east trending regional faults, such as the Variscan Finne–Gera–Jachymov Fault Zone, to which the Kyffhäuser Fault belongs (Bankwitz *et al.*, 1993). A tectonic perturbation is additionally supported by the appearance of poorly rounded detrital zircons among heavy mineral associations from the base of unit c (Schirmer, 1975). From unit f onward, sand-bed braided rivers resembling late phase 1 again prevailed by deposition of the sandy bedform association, indicating a reorganization of the river system at low slope gradients.

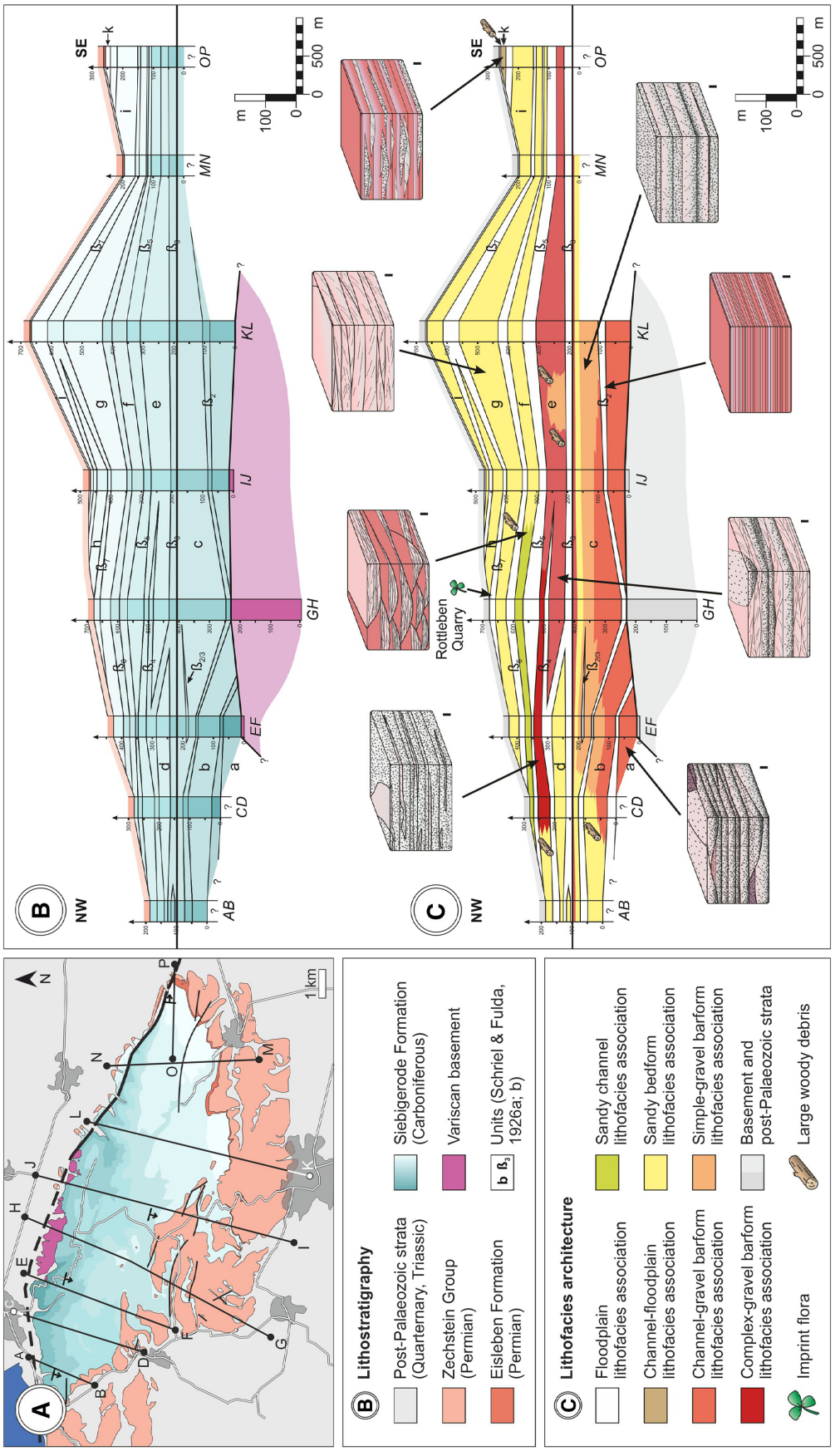

Fig. 12. Lithofacies architecture of the Siebigerode Formation at the Kyffhäuser. The stratigraphic occurrence of lithofacies associations was mapped in eight profiles (AB to OP), each being orientated parallel to the local dip of the strata – for the position of the profiles in the field see (A). (B) and (C) show their lateral correlation in a north-west/south-east direction with the base of unit β_3 being chosen as the main correlative surface.

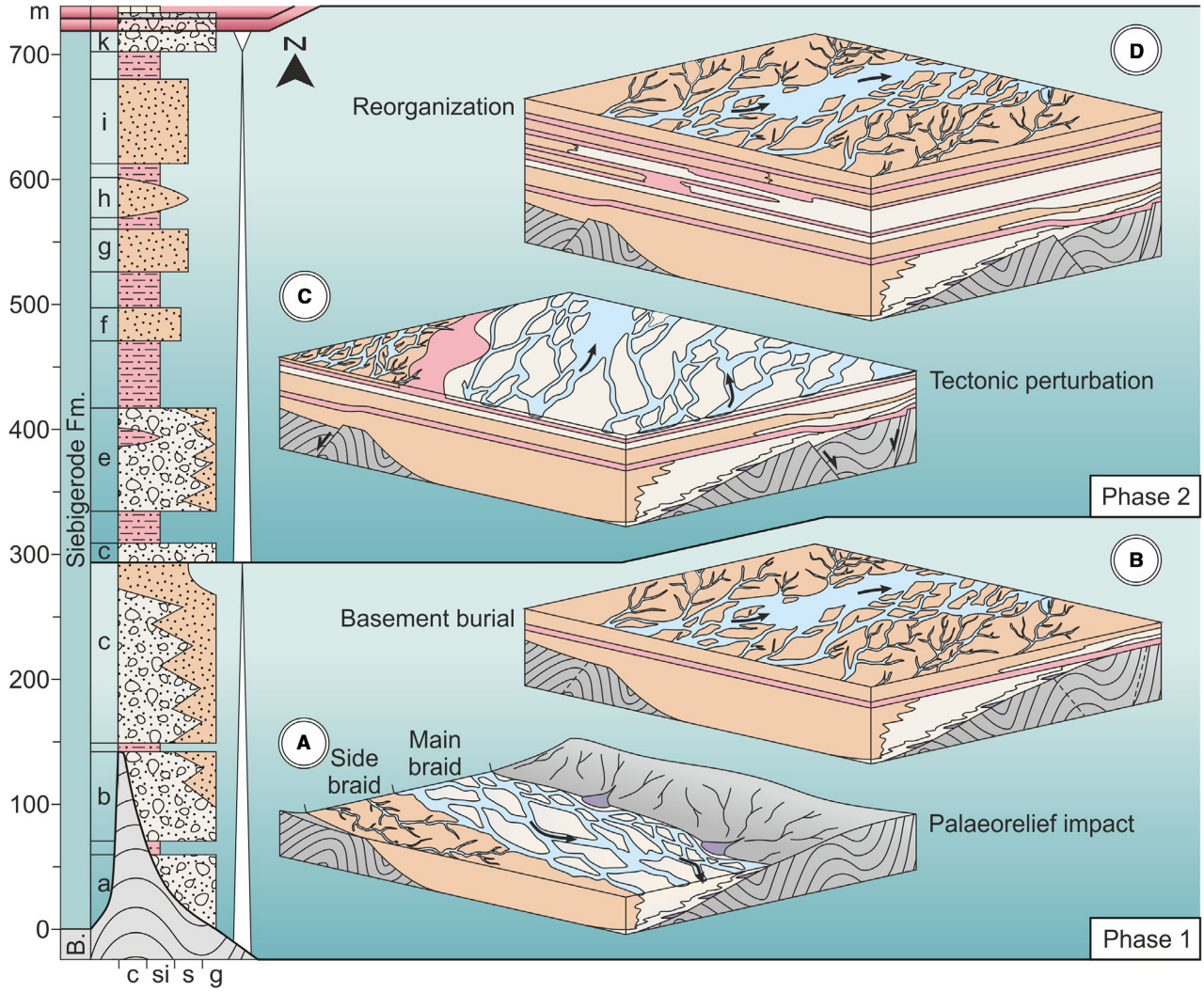

Fig. 13. Two-phase evolution of the Kyffhäuser fluvial system. Section and subdivision according to Schriel & Fulda (1926a,b), adapted and supplemented. Note the phase boundary to be stratigraphically located within unit c. (A) Early phase 1 comprising deposition by a braided river laterally prograding onto a basement elevation during aggradation. Situation reconstructed for unit b. (B) Late phase 1 showing a sand-bed braided river system after basement burial. Note the shift in the transport direction. Situation reconstructed for middle to upper unit c. (C) Early phase 2 initiated by synsedimentary faulting due to crustal relaxation. Perturbation of the fluvial system leads to lithofacies gradients, increased stream competence and an eastward shift of the local subsidence centre. Situation reconstructed for units d+e. (D) Late phase 2 based upon the reorganization of a sand-bed braided river system. Situation reconstructed for unit g.

FOSSIL WOOD ANALYSIS

Obtaining and assessing allometric data

Except for one rootstock, 1·3 m in diameter, petrified woods predominantly occur as horizontally aligned, <20 m long straight trunks lacking roots and branches (Fig. 14A to E). Trunk terminations were broken prior to burial (Fig. 14F). Diameters of trunks being complete in the transverse section do not exceed 91 cm compared to 50 to 100 cm previously reported (Charpentier, 1778; Leonhard, 1831; Göppert, 1864; Mägdefrau, 1958). Vertical compaction is in the range of 35 to 70% (Table S1). Two logs represent basal stem parts being complete in diameter (Fig. 14C and E) and, thus, allow calculations of their original tree heights, which are 35·31 m and 37·34 m, respectively (Table S1).

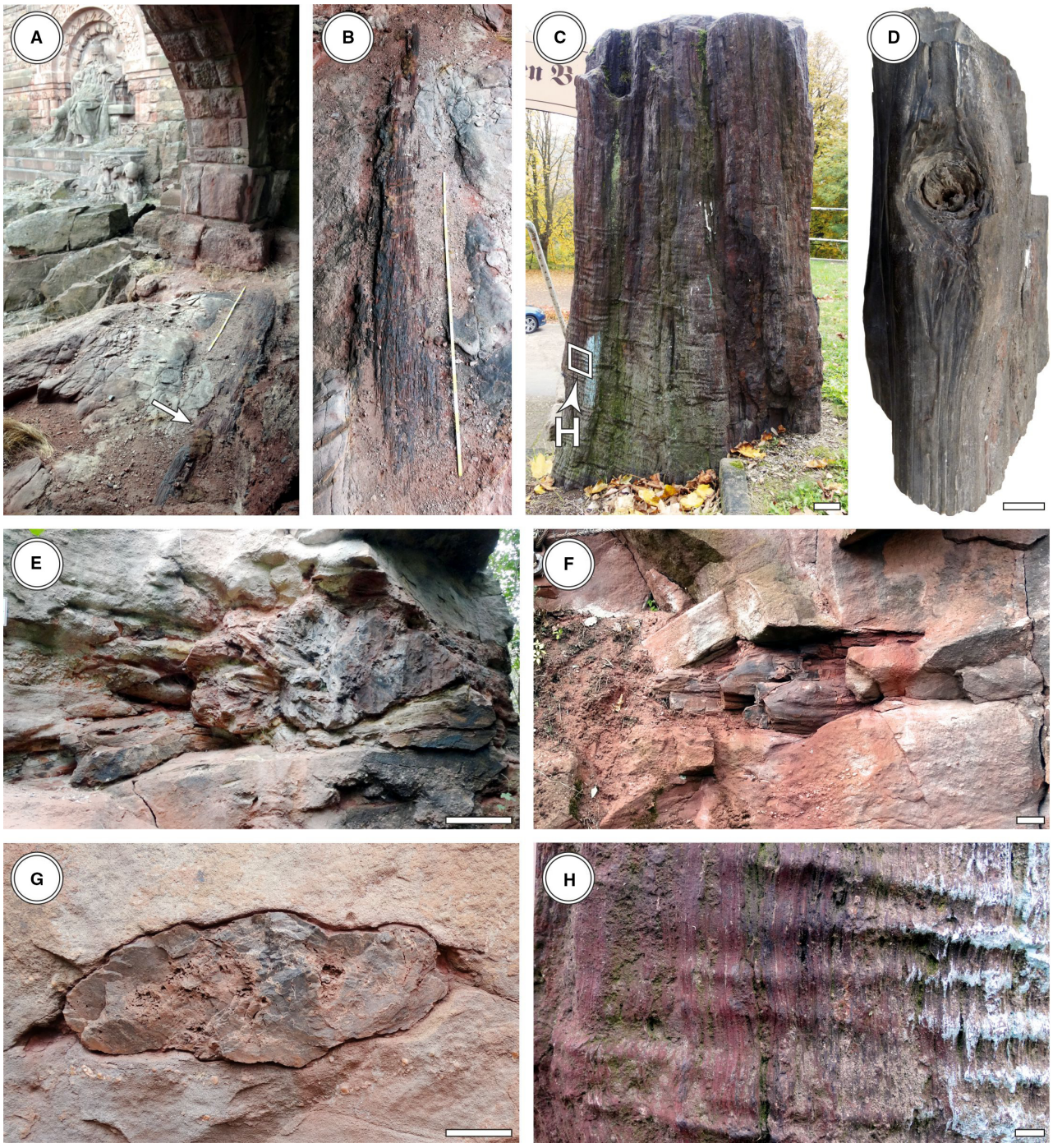

Fig. 14. Large woody debris (LWD) morphology. (A) Trunk (arrow) horizontally embedded in sandstones of the multiple-element lithofacies association (LFA) (Scale: 1 m). (B) Detail of (A). (C) Basal part of a petrified log (Scale: 10 cm). (D) Branch trace in a log fragment (I-446, coll. RMBF, Scale: 1 cm). (E) Rootstock (Scale: 50 cm). (F) Broken termination of a log (Scale: 10 cm) (G) Oval transverse section of a log (Scale: 10 cm). (H) Detail of (C) showing reaction wood, whose formation was connected to loading of superjacent parts of the stem (Scale: 1 cm).

Wood anatomical characteristics

Tissues and systematics

Petrified trunks from the Kyffhäuser mostly lack extra-xylary tissues, except for relics rarely found in branch scars. The *Agathoxylon* wood (Rößler *et al.*, 2014) consists of 30 to 50 μm wide tracheids showing a polygonal to sub-circular outline in cross-section (Fig. 15A). In

tangential longitudinal sections, uniseriate to biseriate rays were documented (Fig. 15B). Pith tissues are replaced in many cases by coarse-crystalline quartz. If preserved, the pith occurs in two types: (i) the regularly chambered cordaitalean *Artisia* type (Fig. 15D and E), whose identification is additionally based upon attached cordaitalean wood; and (ii) the coniferopsid *Tylodendron* type (Fig. 15F), in which sclerenchyma nests <1 mm in diameter occur in the pith parenchyma (Fig. 15G). Branching patterns likewise reveal the presence of cordaitaleans and conifers. Whereas cordaitaleans are represented by sparsely branching long logs or samples containing paired branch traces, conifers possess branches arranged in pseudowhorls (Fig. 15H). However, the morphology of most trunks (branchless straight logs of several metres in length) indicates a higher abundance of cordaitaleans.

Growth increments and event rings

A few specimens exhibit indistinct tree rings (Fig. 15I) 1·5 to 7·0 mm wide. Two event rings *sensu* Luthardt *et al.* (2017) were observed in one cordaitalean (Fig. 16A and B). Both are accompanied by thin callus layers (Fig. 16C to F). The first inner event ring is circumferentially developed and accompanied by a 200 μm thick wood layer on its inner side showing thickened cell walls and diminished cell diameters (Fig. 16A and C). Both the medial and lateral wood–callus transitions are gradual (Fig. 16D). In contrast, the outer event ring does not circle the stem and the wood on its medial side lacks any variation in cell size and cell wall thickness (Fig. 16A, E and F). The medial wood-callus transition is distinct but irregular, whereas the lateral one is gradual (Fig. 16F). Tracheids bordering the medial wood–callus transition are neither disrupted nor deformed. Both growth and event rings either are superimposed by shearing zones or facilitated the formation of concentric fractures subsequently filled by milky quartz (Fig. 16C and E).

Abrasion and decomposition

Abrasive features are widespread among the Kyffhäuser woods. Trunks reveal broken terminations (Fig. 14F) and the wood may be laterally truncated (Fig. 16A and B). Fractures are filled by both sand grains and coarse-crystalline clear quartz (Fig. 16A, B and G). Where anatomically preserved, many fossil woods reveal decomposition of tissues, i.e. isolated, plastically deformed and only faintly preserved tracheids (Fig. 16H).

Impacts of petrifaction

Wood petrifaction was predominantly promoted by silica; hematite forms a minor component (Fig. 17). Specimens showing uniform preservation of their tissues are extremely rare. Anatomical preservation shows considerable spatial variation within a single specimen (Fig. 17A and B) and has been referred to as 'pointstone preservation' in previous studies (Cotta, 1832; Mickle & Barthel, 1992). Wood cells are preserved in selective petrifaction domains exhibiting an irregular to commonly spot-like shape in cross-section (Fig. 17B to E), as opposed to a more band-like appearance in longitudinal sections (Fig. 17F). Accordingly, a tubular three-dimensional geometry of these domains orientated parallel to the tracheids is reconstructed (Fig. 17G). Aside from petrifaction domains, tissues are inadequately preserved, or even completely replaced by coarse-crystalline quartz (Fig. 17D to G). Euhedral quartz blades radially surround the petrifaction domains and contain plastically deformed cells (Fig. 17E to G). These quartz crystals may also occur in isolation accompanied by displacements of neighbouring tissues (Fig. 17H). Hematite either petrified tissues on a broad scale (Fig. 17C and H) or formed sub-millimetre thick coatings on the petrifaction domains (Fig. 17D). However, hematite occurrence is always restricted to areas in which tissues are poorly preserved or even lost.

DISCUSSION

Constraints on large woody debris occurrence and preservation

The isolated occurrence of petrified trunks and their persistent orientation sub-parallel to palaeoflow indicate an uncongested transport of trunks in the Kyffhäuser fluvial system (Braudrick *et al.*, 1997; Gastaldo, 2004). This assessment is strengthened by the fact that dense log jams are completely absent in the Kyffhäuser section despite the presence of large potential obstacles, such as rootstocks (see Bocchiola *et al.*, 2006; Gastaldo & Degges, 2007). Parameters being responsible for whether logs are transported in congested or uncongested

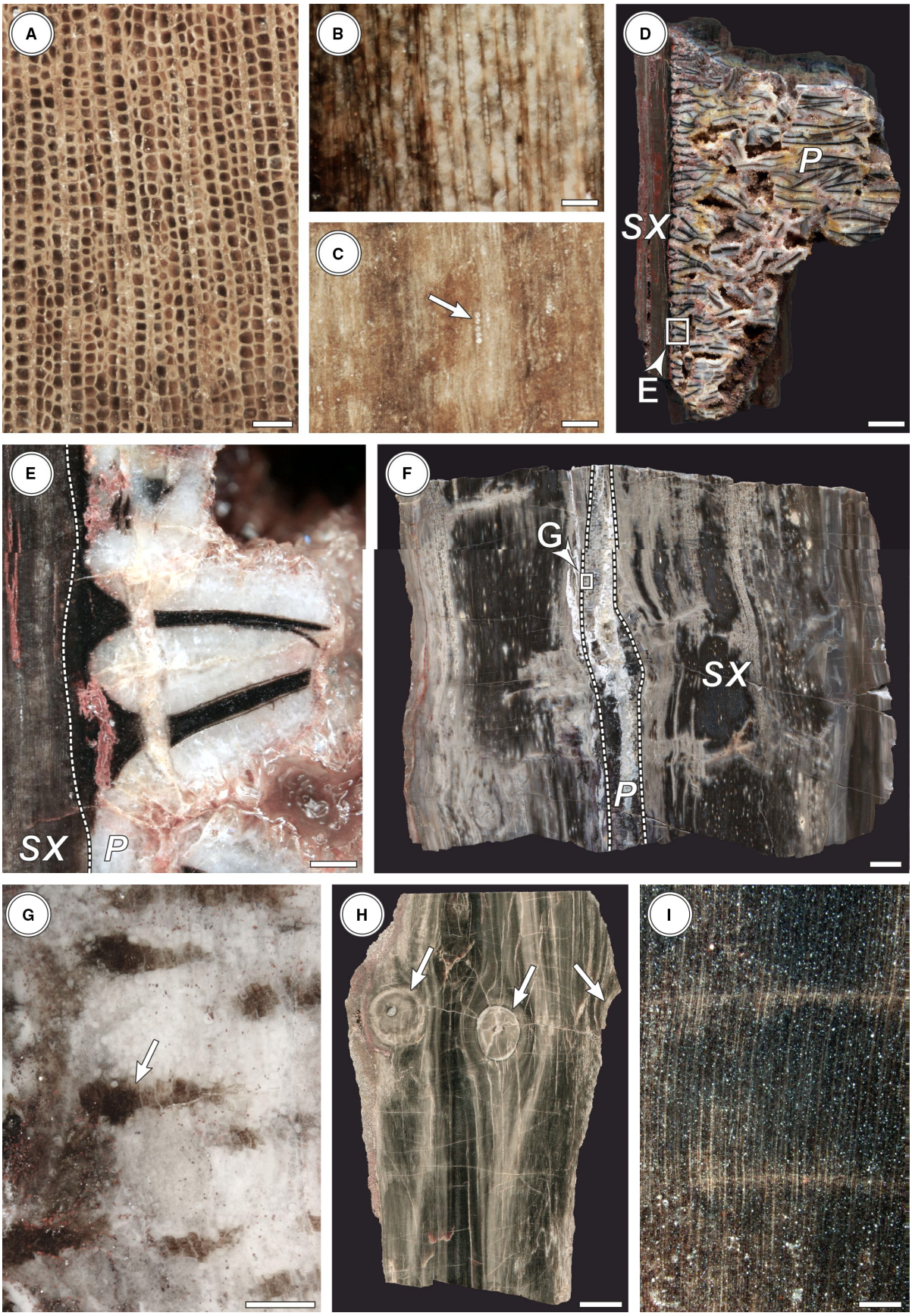

Fig. 15. Large woody debris (LWD) anatomy and systematics. Abbreviations: P: pith, SX: secondary xylem (wood). (A), (B) and (C) *Agathoxylon*-type wood in cross-section [(A) Kyf10, coll. BS], tangential longitudinal section [(B) Kyf151, coll. BS] and radial longitudinal section [(C) WG190a, coll. NMSBS – Scales: 100 μm]. Note uniseriate rays (B) and uniseriate pitting on radial tracheid walls (C). (D) Cordaitalean stem in radial longitudinal section showing the *Artisia*-type pith surrounded by secondary wood (Scale: 1 cm). Note collapsed diaphragms in the pith (Kyf150, coll. BS). (E) Detail of (D) displaying parenchymatic diaphragms extending from the pith-wood interface (Scale: 1000 μm). (F) Conifer stem in radial longitudinal section showing the *Tylodendron*-type pith surrounded by secondary xylem (Kyf151, coll. BS, Scale: 1 cm). (G) Detail of (E) displaying sclerenchyma nests (arrows) in the pith parenchyma (Scale: 500 μm). (H) Pseudowhorl of a conifer stem in a tangential longitudinal section containing three branch traces (arrows, Scale: 1 cm) (Kyf152, coll. BS). (I) Tree rings in K6425b (Scale: 1 mm).

states comprise: (i) the relation of log length and channel width (Braudrick & Grant, 2001; Gurnell *et al.*, 2002); and (ii) the ratio of log input and discharge (Welber, 2013). In the Palaeozoic, the latter ratio is, even more than in the Holocene, constrained by density and composition of the vegetation in the source area providing large woody debris (LWD) (Capretz & Rohn, 2013; Gibling *et al.*, 2014). Lithofacies analysis revealed a broad main braid and high discharges in the Siebigerode Formation, thus favouring an uncongested movement of logs. Similar tendencies in LWD transport have been reported from some modern rivers (Braudrick *et al.*, 1997; Braudrick & Grant, 2001).

The limitation of fossil trunk occurrence to lithofacies architectures containing sandy bedforms and sand bars reflects a restriction of LWD entombment to fluvial regimes, in which water flow deposition either prevailed or at least temporarily occurred (i.e. the side braid). However, given the amount and frequency by which trunks were transported in the Kyffhäuser fluvial system, a primary absence of LWD in the main braid is implausible. Accordingly, the question is raised of which conditions ensure that trunks were remobilized in the main braid rather than in the sandy side braids? According to Buxton (2010), the remobilization of LWD depends on the net force applied to the trunk and results from two retaining and two driving forces. Retaining forces are represented by a friction force (F_F) connected to bed roughness plus the size of the wood-bed contact surface, and a gravitational force (F_G) depending on wood density and size. Both are opposed by a lift force (F_L) connected to buoyancy and, thus, fluid density, and the drag force (F_D) determined by stream velocity. Because fossil wood morphology is uniform in the Kyffhäuser section, the impact of any retaining force connected to wood weight and surface (F_G and F_F) was similar in both the side braid and the main braid. Wood buoyancy in the water certainly remained constant in the whole river, excluding F_L as a reason. The drag force (F_D), however, was likely higher in the main braid, where stream velocity during high discharge was higher than in the side braid. Consequently, LWD on average possessed short residence times in the main braid and was only buried there if woods possessed roots favouring anchoring (Figs 11E to G). Braudrick & Grant (2000) and Curran (2010) found that LWD stability is increased in presence of a rootstock.

Another reason, which has possibly favoured the preservation of LWD in the Siebigerode Formation, is the discharge variability. Based on sediments from modern and ancient river systems, Fielding *et al.* (2009, 2018) found lithofacies architectures in sandy rivers to be shaped considerably by the scale of inter-annual variations of fluvial discharge. Accordingly, if the latter increases, macroform structures become indistinct or are even absent, and deposits connected to critical/supercritical flow conditions gain importance. In the Kyffhäuser, macroforms are indistinctly or rarely preserved in the sandy side braid, and corresponding deposits document a broad range of flow styles. Lithofacies patterns in the sandy side braid, hence, resemble those being typical for intermediate to high discharge variance alluvial deposits *sensu* Fielding *et al.* (2018). Under such hydrological conditions, the entombment of plants both as debris and *in situ* is enhanced.

Silicification of the Kyffhäuser trunks started shortly after burial and took place as a two-phase process (Trümper *et al.*, 2018). The petrifaction domains (Fig. 17D and G) represent the initial phase and display yellow cathodoluminescence resulting from conditions of rapid silica precipitation and oxygen depletion (Götze *et al.*, 2015; Trümper *et al.*, 2018). The wood surrounding the domains was affected later by silicification leading to advanced decomposition, wood displacement or inclusion by quartz crystals and

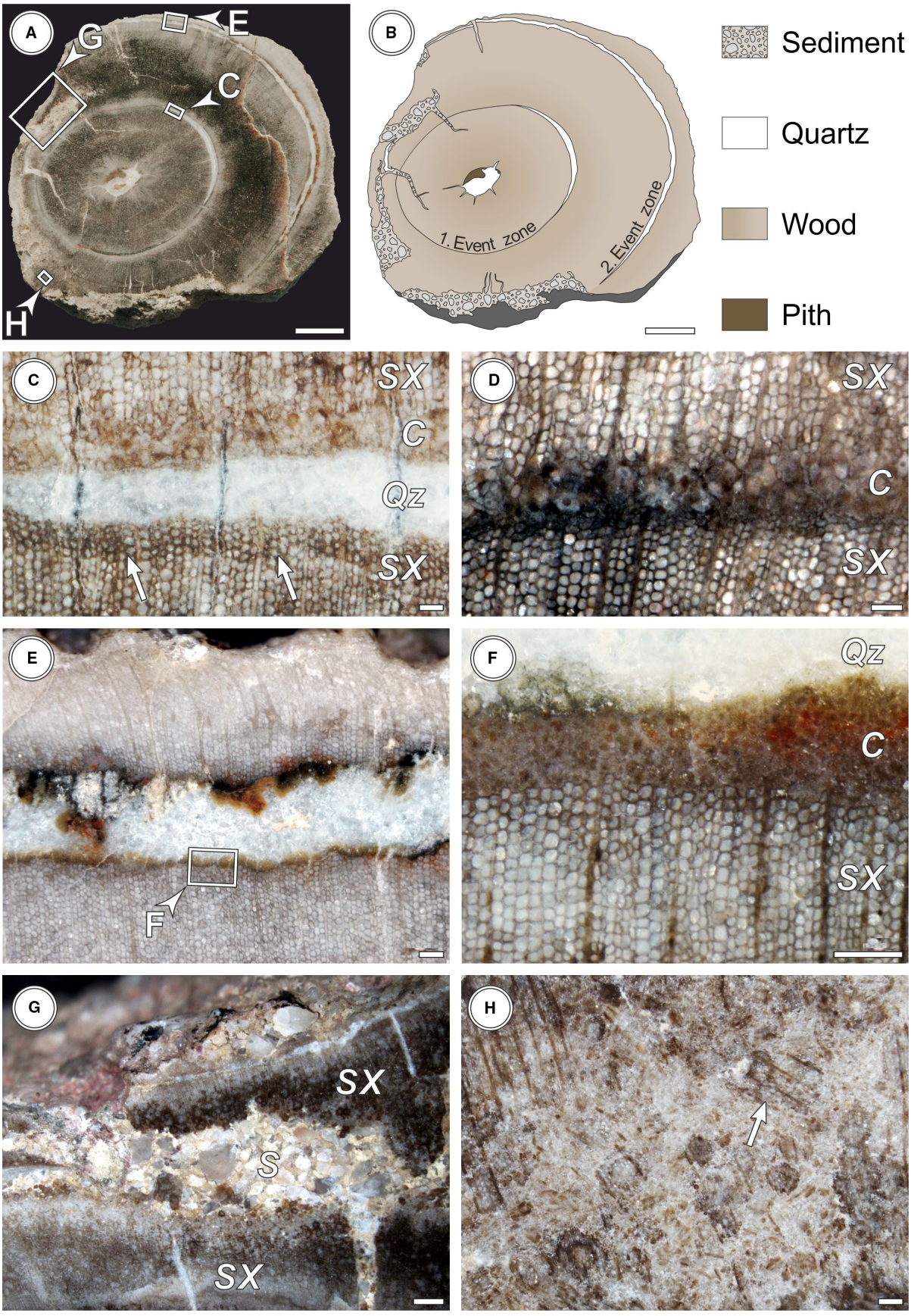

Fig. 16. Event rings and wood decomposition (K134c, coll. MfNC). Abbreviations: C: callus, Qz: quartz, S: sandstone, SX: secondary xylem. (A) Sample K134a, coll. MfNC (Scale: 1 cm). (B) Abstract graph of (A). (C) Inner event ring widened by quartz. Note suddenly increasing cell wall thickness and decreasing cell diameter in the wood towards the event ring (arrows, scale: 100 μm). (D) Inner event ring showing gradual transitions to the neighbouring wood (Scale: 100 μm). (E) Outer event ring (Scale: 200 μm). (F) Detail of (E) showing intact tracheids at the wood–callus interface (Scale: 200 μm). (G) Wood decomposition. Note the displacement of tracheid bundles (arrows, scale: 1 mm). (H) Wood abrasion and injection of sediment (Scale: 200 μm).

compaction of the trunks (Figs 14G, 16H and 17H; Weiss, 1998). According to Trümper *et al.* (2018), these areas exhibit blue cathodoluminescence being typical of a hydrothermal origin (Götze *et al.*, 2001). Franzke *et al.* (2007) stated hydrothermal quartz–hematite mineralization accompanying deposition of the Siebigerode Formation. Given that hematite occurrence is restricted to hydrothermally silicified wood (Fig. 17C, Trümper *et al.*, 2018), final silicification of the Kyffhäuser trunks is suggested here as being connected to this mineralization phase. Diagenetic or hydrothermal overprint of the sediment was additionally recorded by abundant corrosion and hydrothermally altered reaction rims of quartz grains and possibly intergranular dickite (Fig. 5C and D; Trümper *et al.*, 2018).

Trunk provenance and palaeoecological implications

In general, LWD provenance in fluvial deposits is mostly ambiguous depending on how long suspension-load transport and abrasion, or the interaction of these two mechanisms, took place over time. Because LWD accumulations represent time-averaged assemblages, their various wood recruiting processes, such as tributary and alluvial input, forest fire, windthrow, cut bank erosion, flooding (Gurnell, 2013) and their relative proportions cannot be estimated with accuracy. However, profound knowledge of the sedimentary setting and the taphonomy of transported logs is capable of shedding light on these processes and wood provenance (e.g. Bashforth *et al.*, 2014). The Kyffhäuser fluvial system obtained a basin-marginal position and – in case of the lower part of the section – was even directly flanked by basement elevations (Fig. 13A). Fossil logs, hence, were recruited in the study area and/or realms further upstream, both of which include riparian and extra-basinal ('upland') settings; but which of the two latter, or even both, represented the habitats for the trees providing LWD?

Concerning trunk provenance, ambivalent evidence is provided by the Kyffhäuser sediments. One the one hand, it was the dynamic character of fluvial sedimentation being largely inconvenient for long-term growth of up to 40 m tall gymnosperms and, thus, indicating a non-riparian origin. Lithofacies architectures prove deposition of the Siebigerode Formation at the Kyffhäuser by large-scaled, highly dynamic and energetic, aggrading gravel to sand-bed braided rivers, which faced intermediate to high discharge variability. The proportion of coarse-clastics versus fine-clastics in the section (Fig. 12C) indicates that channel deposition prevailed, and voluminous floods carrying sediments and woods were common, as evidenced by successions of up to 2 m thick gravel barforms and sheets (Fig. 8A). The 1·5 m thick inversely graded conglomerates (Fig. 4E) testify to reworking of fluvial sediments. The close succession of deposition and reworking of gravels and sands in the channels was accompanied by the accumulation of fine-sandy silts in the corresponding, elevated floodplains. In the latter areas, the rate of sedimentation apparently was high enough to commonly outperform pedogenesis recorded by rare and immature Calcisols and Vertisols (the only two occurrences of palaeosols in the whole section; Fig. 3A and B). Together with the small thickness and low proportion of floodplain deposits in the Kyffhäuser, especially in the lower part of the section, overbank environments probably represented short-lived, vibrant settings. Given the dynamic fluvial deposition, the rare occurrence of delicate root impressions in the floodplain sediments is suggested to indicate scarce vegetation. A poorly preserved imprint flora gained from clayish siltstone underlying a tuff bed in unit β_7 provides insights into these floodplain communities. The fossil assemblage is dominated by highly fragmentary remains including cordaitalean leaves and pinnae of the pteridosperm *Dicksonites pluckenetii* (Schlotheim ex Brongniart) Sterzel. Tiny pecopterids, odontopterids,

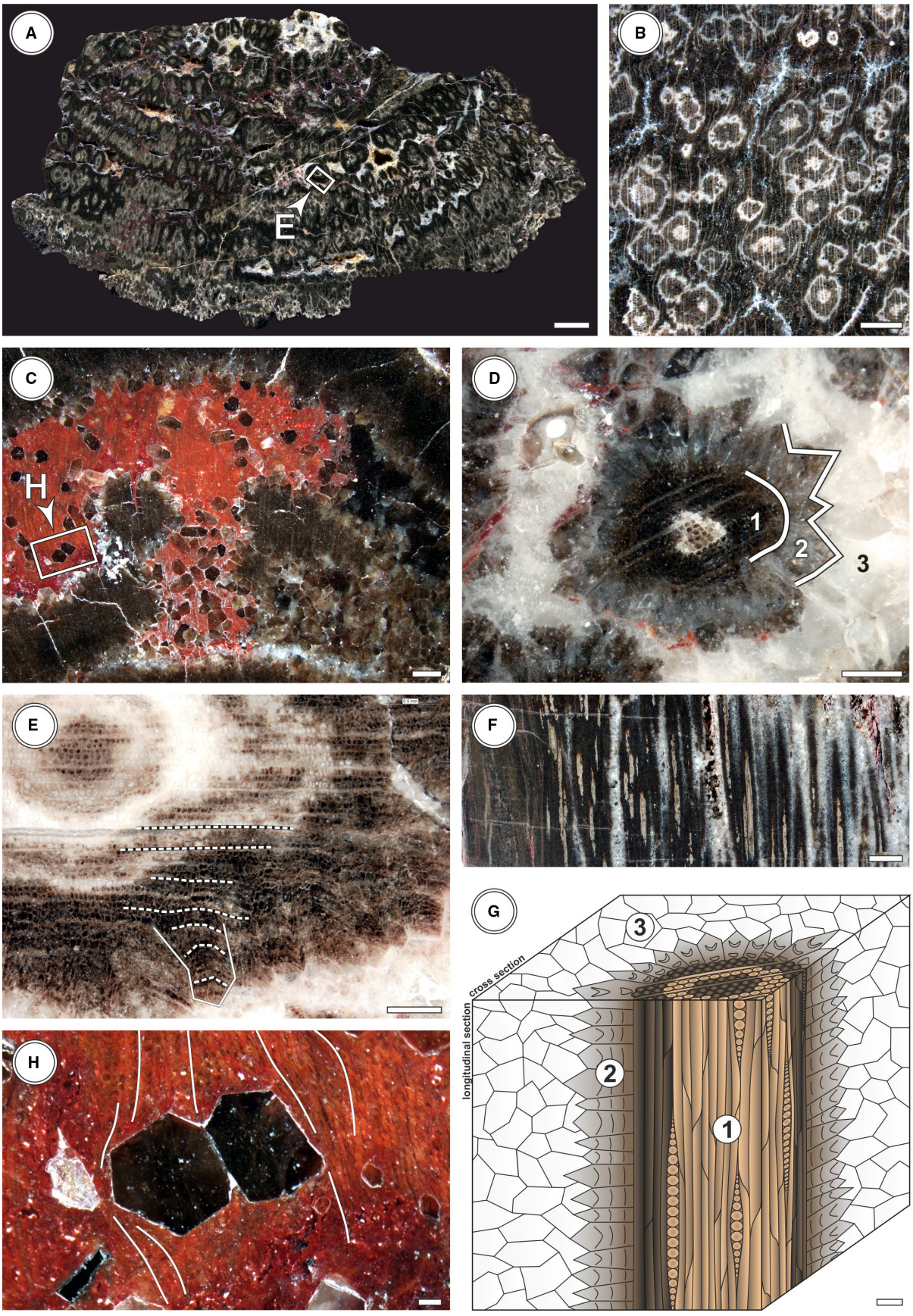

Fig. 17. Impacts of wood petrifaction. (A) Cross-section of K6525 exhibiting spot-like petrifaction domains ('pointstone preservation', Scale: 1 cm). (B) Detail of 'point preservation' (K6226, coll. MfNC, Scale: 1000 μm). (C) Cross-section of K6425b showing irregularly shaped petrifaction (Scale: 1000 μm). (D) Detail of a spot-like petrifaction domain consisting of undeformed silicified tissues (1), surrounded by radially aligned quartz blades (2) and coarse-crystalline quartz (3) (K6426, coll. MfNC, Scale: 500 μm). (E) Plastically deformed wood at the margin of a spot-like petrifaction domain (Scale: 500 μm). (F) 'Pointstone preservation' in longitudinal section (K2097a, coll. MfNC, Scale: 500 μm). (G) Three-dimensional geometry of petrifaction domains (Scale: 100 μm). (H) Displacement of wood by euhedral quartz crystals (K6425b, coll. MfNC, Scale: 100 μm).

Asterophyllites-type leaves, calamitalean stem or pith casts and fragments of walchian conifers were rarely documented (Schriel & Fulda, 1926b; Remy & Kampe, 1961; and recent findings by the present authors). Although this plant assemblage is probably taphonomically biased and contains both parautochthonous and allochthonous elements (for example, conifers), the abundance of up to 10 cm long pinnae of *D. pluckenetii* likely indicates that this plant has rapidly colonized the floodplains. Galtier & Béthoux (2002) found the commonness of this taxon in fluvial deposits of the Graissessac Basin to reflect dense, monospecific stands of scrambling plants, which probably also applied to the Kyffhäuser.

One the other hand, however, a riparian provenance of the fossil logs is inferred from the large proportion of cordaitalean foliage in the aforementioned impression flora, together with the abundance of cordaitalean trunks among the LWD assemblages. This model is further supported by the presence of a fossil rootstock (Fig. 11E to G), which entered the fluvial system most likely via cut-bank erosion (Ash & Creber, 2000; Falcon-Lang & Bashforth, 2010).

Aside from riparian and extra-basinal habitats, another setting being transitional between the two realms fits the controversial arguments and the proposed depositional model better. As reconstructed for the Kyffhäuser (Fig. 13A), the fluvial system was flanked by gentle basement slopes during the burial of a palaeorelief. In contrast to the frequently violated floodplains and channels, such semi-riparian settings represented opportune growth habitats for woody gymnosperms due to depositional quiescence. In the upper reaches of modern medium-scale and large-scale rivers of the Alps, woods are mainly recruited through the following processes: alluvial influx, slope and bank failures and, if present, flooding of vegetated islands (Nakamura & Swanson, 1993; Ruiz-Villanueva *et al.*, 2014; Henshaw *et al.*, 2015). In the Kyffhäuser, an alluvial impact on deposition can be inferred from debris flows in lithofacies associations bordering against the basement (Figs 4G and 7G). Forested islands and bars, however, do not apply to the Kyffhäuser depositional environment, albeit that their absence in upstream reaches cannot be concluded. Hence, at the study site, the authors suggest that large cordaitalean and conifer woods have been obtained from forests covering basement slopes down to the river level. In these habitats, the trees faced seasonally changing water availability as evidenced by tree rings (Fig. 15I), and additionally supported by fluvial architecture and palaeosols of the Siebigerode Formation. Considering this background, event rings (Fig. 16) may be attributed to droughts and fires or display wood responses to fungal attacks (Schweingruber *et al.*, 2006; Luthardt *et al.*, 2017). Floodplains, by contrast, harboured scarce vegetation comprising quickly growing, pioneering plants and maybe young or shrub-like cordaitaleans but did not represent the recruitment areas for LWD.

Large woody debris preservation in Variscan basins

The late Palaeozoic record of anatomically preserved wood reflects a broad range of depositional settings comprising alluvial, fluvial, lacustrine, palustrine and volcanic environments (Trümper *et al.*, 2018). However, numerous Variscan perimontane and intramontane basins across Western and Central Europe yield considerable accumulations of large silicified woody debris embedded in thick fluvial red bed successions of Late Pennsylvanian ('Stephanian') age (Schneider *et al.*, 2006; Fig. 18A). These include the Siebigerode Formation of the Saale Basin (e.g. Mägdefrau, 1958), the Ludwikowice and Odolov formations in the Polish and Czech parts, respectively, of the Intra-Sudetic Basin (e.g. Opluštil *et al.*, 2017), the Štikov Arkoses from the Kumburk Formation of the Krkonoše

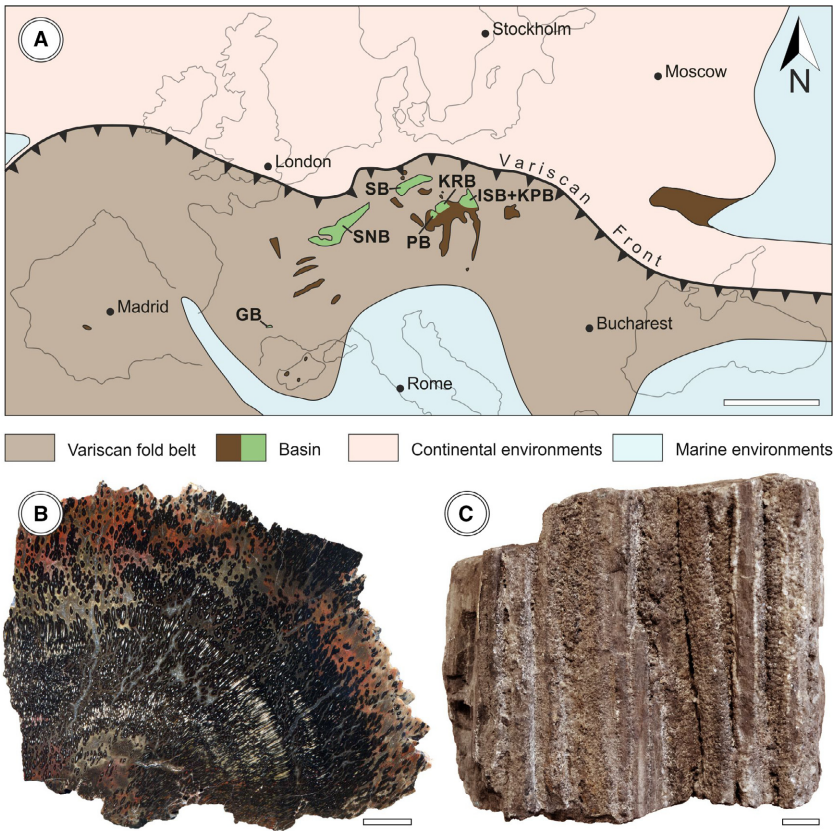

Fig. 18. Distribution of petrified large woody debris occurrences in the Late Pennsylvanian of Europe. (A) Variscan basins providing large woody debris (LWD) hosting Stephanian successions of fluvial origin. Abbreviations: GB: Graissessac Basin; ISB: Intra-Sudetic Basin; KPB: Krkonoše Piedmont Basin, KRB: Kladno-Rakovník Basin, PB: Pilsen Basin, SB: Saale Basin, SNB: Saar-Nahe Basin (modified after Roscher & Schneider, 2006; Scale: 500 km). (B) Petrified wood in cross-section from Nová Paka, Krkonoše Piedmont Basin, Czech Republic (MfNC K5271b; Scale: 1 cm). Note abundant hematite. (C) Petrified wood in lateral view from Nowa Ruda, Intra-Sudetic Basin, Poland (MfNC K2207; Scale: 1 cm).

Piedmont Basin (Mencl *et al.*, 2013; Opluštil *et al.*, 2016b), the Týnec and Líně formations of the Kladno-Rakovník and Pilsen basins (Opluštil *et al.*, 2005, 2016a), the Heusweiler Formation of the Saar-Nahe Basin (e.g. Weithofer, 1897), and the Graissessac Formation of the Graissessac Basin (Galtier *et al.*, 1997). The host rocks represent arkosic sandstones and conglomerates with subordinate floodplain fines deposited by braided rivers. The LWD assemblages are of low diversity and comprise cordaitalean-dominated and/or conifer-dominated assemblages derived from (semi-)riparian settings (Matysová *et al.*, 2010; Mencl *et al.*, 2013). Because of its characteristic appearance, geologists from the 19th century have employed this LWD facies as a lithostratigraphic tool for correlations (Göppert, 1858; Fritsch, 1888; Gaitzsch, 2001) – an approach, which was confirmed later by holostratigraphic correlations (Roscher & Schneider, 2006; Schneider *et al.*, 2006, 2015). Accordingly, stratigraphic occurrences of the aforementioned LWD localities are predominantly limited to the Late Pennsylvanian wet phases B and C; with minor occurrences in the dry interval. The LWD accumulations resembling those of the Stephanian are not documented in both older and younger deposits in Europe raising the question of which circumstances favoured their formation during the Late Pennsylvanian in the Variscan realm.

From the late Moscovian onward, the tropical ever-wet biome of central Pangaea faced increasing aridity, first resulting in seasonally dry conditions in the Late Pennsylvanian and early Permian and culminating in seasonally wet conditions in the middle and late Permian (Chumakov & Zharkov, 2002; Roscher & Schneider, 2006). However, late Palaeozoic aridification was not a linear process; rather, it represented a time-averaged development consisting of an alternation of wet and dry phases (Roscher & Schneider, 2006; Tabor & Poulsen, 2008; Montañez & Poulsen, 2013; Fig. 2). Climatic oscillations influenced depositional environments in central Pangaea, as revealed by the geological record (Roscher & Schneider, 2006; Opluštil & Cleal, 2007; Lojka *et al.*, 2009; DiMichele *et al.*, 2010; Looy *et al.*, 2014). Focusing on the Late Pennsylvanian, climatic impacts on fluvial discharge and deposition determined the potential for LWD preservation (Fielding *et al.*, 2018). Fluvial sediments formed during the wet phase B (the Siebigerode Formation, this study)

exhibit lithofacies patterns pointing to braided river systems prone to frequent avulsion, deposition and less ephemeral channel flow (Bristow & Best, 1993). Under such depositional conditions, trunks were quickly buried and frequent flooding increased LWD supply, as inferred from recent fluvial systems (Gurnell *et al.*, 2002). In contrast, sediments from the Late Pennsylvanian dry interval (for example, the Stephanian B Rothenburg Formation of the Saale Basin, Gebhardt & vHiete, 2013; Fig. 2) reveal a much more ephemeral and sediment-laden fluvial deposition. Deposits show poor sorting and commonly indistinct bedding. Clasts are coated by hematite crusts. Channel elements occur in isolation within thick floodplain successions containing mature Calcisols and lacustrine carbonates (Gebhardt, 1988; Schneider *et al.*, 2005), and consist of fining-upward successions. Avulsion was much more inhibited and fluvial channels frequently fell dry (Gaitzsch, 2001). Compared to the wet phase B Siebigerode Formation, depositional conditions of the dry interval Rothenburg Formation were more suitable for wood decay impeding the ability to accumulate and preserve thick sedimentary successions, including LWD. Additionally, a drier climate probably impeded vegetation development in the source areas leading to reduced wood supply. In the Permian, however, increasing aridity strengthened fluvial ephemerality and further reduced the potential for LWD transport and preservation in the Central European part of the Variscides. Consequently, alluvial and volcanic environments became increasingly important in preserving woods during the latest Palaeozoic (Trümper *et al.*, 2018).

Large woody debris preservation in Late Pennsylvanian intramontane basins seems also to have been related to the Pennsylvanian/Permian vegetational turnover in central Pangaea. Initiated by Variscan tectonics and subsequent climatic change, gymnosperm-dominated hinterland floras increasingly replaced the basinal wetland floras after the late Moscovian (DiMichele & Aronson, 1992; Kerp, 1996; DiMichele *et al.*, 2008; DiMichele, 2014). This process was accompanied by expansion and diversification of gymnosperms, many of them possessing thick woody trunks (Kerp, 1996; Rothwell *et al.*, 1997). Hence, an increasing wood supply to rivers can be concluded for the Late Pennsylvanian. In addition, the formation and rapid erosion of the Variscan Orogen provided voluminous clastic material, which accumulated in nearby basins (Fig. 18A). Wood recruitment probably also benefited from the relatively small size of the Variscan basins. Based on multiple lines of evidence from Euramerica, Kerp (1996) underlined the increasing proportion of mesophilous to xerophilous elements among floral assemblages with decreasing basin size and, thus, reduced atmospheric humidity.

Finally, emphasis is placed on the importance of late Palaeozoic tectonics in providing accommodation space for the accumulation of thick sedimentary successions. In the Late Pennsylvanian, around 305 Ma, the transition from late-Variscan transpression to post-Variscan extension initiated a striking phase of basin formation (Kroner & Romer, 2013). This process is reflected by the huge stratigraphic records of several intramontane basins across Western and Central Europe starting in the Stephanian (Schneider *et al.*, 2015).

Braided river systems carrying LWD appeared not only in the European part of equatorial Pangaea. Corresponding deposits are also reported from the Early Pennsylvanian of the Sydney and Maritimes basins, Atlantic Canada, where they indicate sparse gymnosperm-dominated forests even in lowland settings (Falcon-Lang, 2006; Bashforth *et al.*, 2014). Hence, the Pennsylvanian represented a time slot for the formation of considerable LWD accumulations, which document the formation of seasonally dry intramontane basins and vegetation turnover in the Variscan realm across a 3000 km distance.

CONCLUSIONS

For 250 years, petrified wood-bearing strata from the Kyffhäuser have attracted attention both in the scientific community and from the general public, and were an object of research among notable palaeobotanists and geologists (Walch, 1771; Charpentier, 1778; Freiesleben, 1793; v. Leonhard, 1831; Cotta, 1832; Göppert, 1880; Mägdefrau, 1958; Mickle & Barthel, 1992). However, a profound understanding of their systematic affinity, origin, palaeoecological and taphonomic significance remained ambiguous until now. By using a multidisciplinary approach, the following deductions are drawn on a local to inter-regional scale:

- Sediments and plant assemblages of the Kyffhäuser section reflect the gradual burial of a Variscan basement elevation by gravel-bed to sand-bed braided rivers in seasonally dry climatic conditions.

- Alluvial influx and cut-bank erosion recruited woods from up to 40 m tall cordaitaleans and conifers which sparsely forested slopes flanking the river system. An uncongested log transport was facilitated by high discharges and the broad width of the river braids.
- The preservation potential of woody debris was constrained by fluvial discharge and morphology, the amount and shape of woods, and aggradation rate. Purely gravel-bar forming environments supported short residence times diminishing trunk fossilization.
- Silicification of the drifted logs affected wood tissues selectively and finished with hydrothermal silica precipitation connected to regional quartz–hematite mineralization.
- During the Pennsylvanian, tectonic basin formation, climate and the diversification of gymnosperms promoted the emergence of large woody debris (LWD) containing river systems in equatorial Pangaea.

ACKNOWLEDGEMENTS

For providing samples making this work possible, we highly acknowledge Matthias Borchardt (Steinthaleben), Alexander Gehler (Göttingen), Ulrich Hahnemann (Bad Frankenhausen), Angelika Hesse (Dessau), Antje Kuchenbecker (Bad Frankenhausen), Paul Meyer (Tilleda), Eberhard Mey (Rudolstadt), Stephan Schultka (Berlin) and Ralf Werneburg (Schleusingen). We are grateful to Ludwig Luthardt, Chemnitz, and Robert Noll, Tiefenthal, for their encouraging discussion on wood anatomy. Further gratitude is attributed to Jens Götze (Freiberg) for supporting the CL analysis and Matthias Franz (Göttingen) in discussing the depositional environment. We are indebted to Sebastian Germann (Freiberg) and Dorothee Mertmann (Halle) for fieldwork assistance. We thank Hans Joachim Franzke (Clausthal-Zellerfeld), Robert A. Gastaldo (Waterville), Alexandra Hellwig (Chemnitz) and Evelyn Kustatscher (Bozen) for fruitful discussions. Catrin Auerbach and Jens Lüdecke (both Kyffhäuser) offered access to crucial outcrops. Special thanks are due to Gudrun Geyer, Michael Magnus (both Freiberg), Mathias Merbitz, Michael Junge (both Chemnitz) and Tristan Roscher (Deutschneudorf) for sample preparation and inventory. We thank reviewers Sylvie Bourquin (Rennes), Christopher J. Cleal (Cardiff), William A. DiMichele (Washington, D.C.), Jean-Francois Ghienne (Strasbourg), Stanislav Opluštil (Prague), three anonymous reviewers and the editor Christopher R. Fielding (Lincoln/Nebraska) for their constructive comments, which considerably enhanced the paper. JWS thanks the Russian Government for a subsidy in the frame of the program 'Competitive Growth of Kazan Federal University among World's Leading Academic Centers'. Our project was funded by the Deutsche Forschungsgemeinschaft (DFG grant RO 1273/4-1 to RR).

REFERENCES

Abbe, T.B. and **Montgomery, D.R.** (1996) Patterns and processes of wood debris accumulation in the Queets River Basin, Washington. *Geomorphology*, **51**, 81–107.

Abbe, T.B. and **Montgomery, D.R.** (2003) Large woody debris jams, channel hydraulics and habitat formation in large rivers. *Regul. Rivers Res. Manag.*, **12**, 201–221.

Alexander, J., **Fielding, C.R.** and **Jenkins, G.** (1999) Plant-material deposition in the tropical Burdekin River, Australia: implications for ancient fluvial sediments. *Palaeogeogr. Palaeoclimatol. Palaeoecol.*, **153**, 105–125.

Allen, J.R.L. (1983) Gravel overpassing on humpback bars supplied with mixed sediment: examples from the Lower Old Red Sandstone, southern Britain. *Sedimentology*, **30**, 285–294.

Ash, S.R. and **Creber, G.T.** (2000) The Late Triassic *Araucarioxylon arizonicum* trees of the Petrified Forest National Park, Arizona, USA. *Palaeontology*, **43**, 15–28.

Baker, C.J. (1979) The laminar horseshoe vortex. *J. Fluid Mech.*, **95**, 347–367.

Bankwitz, P., **Gross, U.** and **Bankwitz, E.** (1993) Krustendeformation im Bereich der Finne-Kyffhäuser-Gera-Jachymov-Zone. *Z. Geol. Wiss.*, **21**, 3–20.

Barthel, M., **Mütze, K.** and **Simon, R.** (1975) Neue Funde fossiler Pflanzen aus dem Saale-Trog. *Wiss. Z. Humboldt-Univ. Math.-Nat. R.*, **24**, 475–485.

Bashforth, A.R., **Falcon-Lang, H.J.** and **Gibling, M.R.** (2010) Vegetation heterogeneity on a Late Pennsylvanian braided-river plain draining the Variscan Mountains, La Magdalena Coalfield, northwestern Spain. *Palaeogeogr. Palaeoclimatol. Palaeoecol.*, **292**, 367–390.

Bashforth, A.R., **Cleal, C.J.**, **Gibling, M.R.**, **Falcon-Lang, H.J.** and **Miller, R.F.** (2014) Paleoecology of Early Pennsylvanian vegetation on a seasonally dry tropical landscape (Tynemouth Creek Formation, New Brunswick, Canada). *Rev. Palaeobot. Palynol.*, **200**, 229–263.

Beyschlag, F. and **Fritsch, K.v.** (1888) Das Jüngere Steinkohlengebirge und das Rothliegende in der Provinz Sachsen und den angrenzenden Gebieten. *Abh. K. Preuss. Geol. Landesanst.*, **10**, 1–263.

Blair, T.C. and **McPherson, J.G.** (1994) Alluvial fans and their natural distinction from rivers based on morphology, hydraulic processes, sedimentary processes, and facies assemblages. *J. Sed. Res.*, **A64**, 450–489.

Bocchiola, D., **Rulli, M.C.** and **Rosso, R.** (2006) Transport of large woody debris in the presence of obstacles. *Geomorphology*, **76**, 166–178.

Braudrick, C.A. and **Grant, G.E.** (2000) Transport and deposition of large woody debris in streams: a flume experiment. *Geomorphology*, **41**, 166–178.

Braudrick, C.A. and **Grant, G.E.** (2001) When do logs move in rivers. *Water Resour. Res.*, **36**, 571–583.

Braudrick, C.A., **Grant, G.E.**, **Ishikawa, Y.** and **Ikeda, H.** (1997) Dynamics of wood transport in streams: a flume experiment. *Earth Surf. Proc. Land.*, **22**, 669–683.

Breitkreuz, C. and **Kennedy, A.** (1999) Magmatic flare-up at the Carboniferous/Permian boundary in the NE German Basin revealed by SHRIMP zircon ages. *Tectonophysics*, **302**, 307–326.

Breitkreuz, C., **Ehling, B.-C.** and **Sergeev, S.** (2009) Chronological evolution of an intrusive/extrusive system: the late Paleozoic Halle Volcanic Complex in the northeastern Saale Basin (Germany). *Z. Dtsch. Ges. Geowiss.*, **160**, 173–190.

Bristow, J.L. and **Best, J.L.** (1993) Braided rivers: perspectives and problems. In: *Braided Rivers* (Eds J.L. Best and J.L. Bristow), *Geol. Soc. Spec. Publ.*, **75**, 1–11.

Buxton, T.H. (2010) Modeling entrainment of waterlogged large wood in stream channels. *Water Resour. Res.*, **46**, W10537.

Capretz, R.L. and **Rohn, R.** (2013) Lower Permian stems as fluvial paleocurrent indicators of the Parnaíba Basin, northern Brazil. *J. S. Am. Earth Sci.*, **45**, 69–82.

Charpentier, J.F.W. (1778) *Mineralogische Geographie der Chursächsischen Lande mit Kupfern*. Verlag Siegfried Leberecht Crusius, Leipzig, 432 pp.

Chumakov, N.M. and **Zharkov, M.A.** (2002) Climate during Permian-Triassic Biosphere Reorganizations, Article 1: Climate of the Early Permian. *Stratigr. Geol. Corr.*, **10**, 586–602.

Cotta, B. (1832) *Die Dendrolithen in Bezug auf ihren inneren Aufbau*. Arnoldische Buchhandlung, Dresden, Leipzig, 89 pp.

Curran, J.C. (2010) Mobility of large woody debris (LWD) jams in a low gradient channel. *Geomorphology*, **116**, 320–329.

Dickinson, W. (1985) Interpreting provenance relations from detrital modes of sandstones. In: *Provenance of Arenites* (Ed. G. Zuffa), pp. 333–362. Nato Science Series, Reidel Publishing Company, Dordrecht.

DiMichele, W.A. (2014) Wetland-dryland vegetational dynamics in the Pennsylvanian ice age tropics. *Int. J. Plant Sci.*, **175**, 123–164.

DiMichele, W.A. and **Aronson, R.B.** (1992) The Pennsy lvanian-Permian vegetational transition: A terrestrial analogue to the onshore-offshore hypothesis. *Evolution*, **46**, 807–824.

DiMichele, W.A., **Kerp, H.**, **Tabor, N.J.** and **Looy, C.V.** (2008) The so-called "Paleophytic–Mesophytic" transition in equatorial Pangea – Multiple biomes and vegetational tracking of climate change through geological time. *Palaeogeogr. Palaeoclimatol. Palaeoecol.*, **268**, 152–163.

DiMichele, W.A., **Cecil, C.B.**, **Montanez, I.P.** and **Falcon-Lang, H.J.** (2010) Cyclic changes in Pennsylvanian paleoclimate and effects on floristic dynamics in tropical Pangaea. *Int. J. Coal Geol.*, **83**, 329–344.

Ehling, B.-C., **Breitkreuz, C.** and **Sergeev, S.** (2005) Improved stratigraphy of the late Paleozoic Halle Volcanic Complex: New SHRIMP U/Pb ages of porphyritic rhyolites. *Schriftenr. dt. geol. Ges.*, **39**, 90.

Falcon-Lang, H.J. (2006) Vegetation ecology of Early Pennsylvanian alluvial fan and piedmont environments in southern New Brunswick, Canada. *Palaeogeogr. Palaeoclimatol. Palaeoecol.*, **233**, 34–50.

Falcon-Lang, H.J. and **Bashforth, A.R.** (2004) Pennsylvanian uplands were forested by giant cordaitalean trees. *Geology*, **32**, 417–420.

Falcon-Lang, H.J. and **Bashforth, A.R.** (2010) Pennsylvanian uplands were forested by giant cordaitalean trees. *Geology*, **32**, 417–420.

Falcon-Lang, H.J. and **Scott, A.C.** (2000) Upland ecology of some Late Carboniferous cordaitalean trees from Nova Scotia and England. *Palaeogeogr. Palaeoclimatol. Palaeo ecol.*, **156**, 225–242.

Ferguson, R.I. and **Werritty, A.** (1983) Bar development and channel changes in the gravelly river Feshie, Scotland. *Spec. Publ. Int. Assoc. Sedimentol.*, **6**, 181–193.

Fielding, C.R. and **Alexander, J.** (1996) Sedimentology of the Upper Burdekin River of North Queensland – an example of a tropical, variable discharge river. *Terra Nova*, **8**, 447–457.

Fielding, C.R. and **Alexander, J.** (2001) Fossil trees in ancient fluvial channel deposits: evidence of seasonal and longer-term climatic variability. *Palaeogeogr. Palaeoclimatol. Palaeoecol.*, **170**, 59–80.

Fielding, C.R., **Alexander, J.** and **Newman-Sutherland, E.** (1997) Preservation of in situ, arborescent vegetation and fluvial bar construction in the Burdekin River of north Queensland, Australia. *Palaeogeogr. Palaeoclimatol. Palaeoecol.*, **135**, 123–144.

Fielding, C.R., **Allen, J.P.**, **Alexander, J.** and **Gibling, M.R.** (2009) Facies model for fluvial systems in the seasonal tropics and subtropics. *Geology*, **37**, 623–626.

Fielding, C.R., **Alexander, J.** and **Allen, J.P.** (2018) The role of discharge variability in the formation and preservation of alluvial sediment bodies. *Sed. Geol.*, **365**, 1–20.

Fossen, H. (2016) *Structural Geology*. Cambridge University Press, Cambridge, 510 pp.

Franzke, H.J., **Zeh, A.** and **Meier, S.** (2007) Die metamorph-magmatische und strukturelle Entwicklung des Kyffhäuser Kristallins/Mitteldeutsche Kristallinzone – Vergleich mit der Wippra-Zone und dem Eckergneis/Harz. *Z. Geol. Wiss.*, **35**, 27–61.

Freiesleben, J.C. (1793) Geognostisch-bergmännische Beobachtungen auf einer Reise durch Saalfeld, Camsdorf und einen Theil Thüringens. *Mag. f. Bergbauk.*, **10**, 3–114.

Fritsch, K.v. (1888) Das Saaletal zwischen Wettin und Cönnern. *Z. Naturwiss.*, **61**, 114–142.

Gaitzsch, B. (2001) Das Oberkarbonprofil der Saale-Senke am Kyffhäuser – Eine Diskussion. *Beitr. Geol. Thür.*, **8**, 43–66.

Gaitzsch, B., **Rößler, R.**, **Schneider, J.W.** and **Schretzenmayr, S.** (1998) Neue Ergebnisse zur Verbreitung potentieller Muttergesteine im Karbon der variscischen Vorsenke in Norddeutschland. *Geol. Jb.*, **149**, 25–58.

Galtier, J. and **Béthoux, O.** (2002) Morphology and growth habit of *Dicksonites pluckentii* from the Upper Carboniferous of Graissessac (France). *Geobios*, **35**, 525–535.

Galtier, J., **Daviero, V.** and **Meyer-Berthraud, B.** (1997) Découverte de fragments de troncs d'arbres perminéralisé dans le bassin Stéphanien de Graissessac (Sud du Massif Central, France). *Geobios*, **20**, 243–247.

Gastaldo, R.A. (2004) The relationship between bedform and log orientation in a Paleogene fluvial channel, Weißelster

Basin, Germany: Implications for the use of coarse woody debris for paleocurrent analysis. *Palaios*, **19**, 587–597.

Gastaldo, R.A. and **Degges, C.W.** (2007) Sedimentology and paleontology of a Carboniferous log jam. *Int. J. Coal Geol.*, **69**, 103–118.

Gebhardt, U. (1988) Mikrofazies und Paläontologie biogener Karbonate der Unteren Mansfelder Schichten. (Oberkarbon, Stefan). *Hall. Jb. Geowiss.*, **13**, 5–21.

Gebhardt, U. and **Hiete, M.** (2013) Continental Upper Carboniferous red beds in the Variscan intermontane Saale Basin, central Germany: orbital forcing detected by wavelet analysis. *Geol. Soc. Spec. Publ.*, **376**, 177–199.

Gibling, M.R., **Bashforth, A.R.**, **Falcon-Lang, H.J.**, **Allen, J.P.** and **Fielding, C.R.** (2010) Log jams and flood sediment buildup caused channel abandonment and avulsion in the Pennsylvanian of Atlantic Canada. *J. Sed. Res.*, **80**, 268–287.

Gibling, M.R., **Davies, N.S.**, **Falcon-Lang, H.J.**, **Bashforth, A.R.**, **DiMichele, W.A.**, **Rygel, M.C.** and **Ielpi, A.** (2014) Palaeozoic co-evolution of rivers and vegetation: a synthesis of current knowledge. *Proc. Geol. Assoc.*, **125**, 524–533.

Göppert, H.R. (1858) Ueber die versteinten Wälder im nördlichen Böhmen und in Schlesien. *Jb. Schles. Ges. f. vaterl. Kultur*, **36**, 41–49.

Göppert, H.R. (1864) *Die fossile Flora der Permischen Formation*. Verlag von Theodor Fischer, Kassel, 484 pp.

Göppert, H.R. (1880) Ueber die versteinerten Hölzer des Kyffhäuser. *N. Jb. Min.*, **1**, 89–92.

Götze, J., **Plötze, M.** and **Habermann, D.** (2001) Origin, spectral characteristics and practical applications of the cathodoluminescence (CL) of quartz – a review. *Mineral. Petrol.*, **71**, 225–250.

Götze, J., **Pan, Y.**, **Stevens-Kalceff, M.**, **Kempe, U.** and **Müller, A.** (2015) Origin and significance of yellow cathodoluminescence (CL) of quartz. *Am. Mineral.*, **100**, 1469–1482.

Graf, W.H. and **Altinakar, M.S.** (2017) Local scour. In: *River System Analysis and Management* (Ed. N. Sharma), pp. 145–166. Springer, Singapore.

Gurnell, A.M. (2013) Wood in fluvial systems. *Treat. Geomorphol.*, **9**, 163–188.

Gurnell, A.M., **Piegay, H.**, **Swanson, F.J.** and **Gregory, S.V.** (2002) Large wood and fluvial processes. *Freshwat. Biol.*, **47**, 601–619.

Henshaw, A.J., **Bertoldi, W.**, **Harvey, G.L.**, **Gurnell, A.M.** and **Welber, M.** (2015) Large wood dynamics along the Tagliamento River, Italy: Insights from Field and Remote Sensing investigations. In: *Engineering Geology for Society and Territory – Volume 3 River Basins, Reservoir Sedimentation and Water Resources* (Eds G. Lollino, M. Arattano, M. Rinaldi, O. Giustolisi, J.-C. Marechal and G.E. Grant), *IAEG XII Congress volumes on the occasion of the 50th anniversary of IAEG*, **3**, 151–154.

Hoyningen-Huene, E.v. (1960) Das Permokarbon im östlichen Harzvorland. *Freib. Forsch.-H.*, **C 93**, 1–116.

Ielpi, A., **Gibling, M.R.**, **Bashforth, A.R.**, **Lally, C.**, **Rygel, M.C.** and **Al-Siwadi, S.** (2014) Role of vegetation in shaping Early Pennsylvanian braided rivers: Architecture of the Boss Point Formation, Atlantic Canada. *Sedimentology*, **61**, 1659–1700.

Joeckel, R.M., **Tucker, S.T.** and **Fielding, C.R.** (2015) Sedimentological effects and stratigraphic implications of a rare, high-stage flow in an evolving, braided to anabranching stream with riparian woodland. *Sed. Geol.*, **325**, 71–89.

Keighley, D.G. and **Pickerill, R.K.** (2003) Ichnocoenoses from the Carboniferous of eastern Canada and their implications for the recognition of ichnofacies in nonmarine strata. *Atlantic Geol.*, **39**, 1–22.

Keller, E.A. and **Swanson, F.J.** (1979) Effects of large organic material on channel form and fluvial processes. *Earth Surf. Proc. Land.*, **4**, 361–380.

Kerp, H. (1996) Post-Variscan late Paleozoic Northern Hemisphere gymnosperms: the onset of the Mesozoic. *Rev. Palaeobot. Palynol.*, **90**, 263–285.

Kroner, U. and **Romer, R.L.** (2013) Two plates – Many subduction zones: The Variscan orogeny reconsidered. *Gondwana Res.*, **24**, 298–329.

Legros, F. (2002) Can dispersive pressure cause inverse grading in grain flows? *J. Sed. Res.*, **72**, 166–170.

Leonhard, K.C.v. (1831) Grundzüge der Geologie und Geognosie. Lehrbuch für öffentliche Vorträge, besonders auch in Gymnasien und Regelschulen, sowie zum Selbststudium, 428 pp.

Lojka, R., **Drábková, J.**, **Zajíc, J.**, **Sýkorová, I.**, **Franců, J.**, **Bláhová, A.** and **Grygar, T.** (2009) Climate variability in the Stephanian B based on environmental record of the Mšec Lake deposits (Kladno–Rakovník Basin, Czech Republic). *Palaeogeogr. Palaeoclimatol. Palaeoecol.*, **280**, 78–93.

Looy, C.V., **Kerp, H.**, **Duijnstee, I.A.P.** and **DiMichele, W.A.** (2014) The late Paleozoic ecological–evolutionary laboratory, a land–plant fossil record perspective. *Sed. Rec.*, **12**, 4–10.

Ludwig, G. (1955) Neue Ergebnisse der Schwermineral- und Kornanalyse im Oberkarbon und Rotliegenden des südlichen und östlichen Harzvorlandes. *Beih. Zeitschr. Geol.*, **14**.

Luthardt, L., **Rößler, R.** and **Schneider, J.W.** (2017) Tree-ring analysis elucidating palaeo-environmental effects captured in an in situ fossil forest – The last 80 years within an early Permian ecosystem. *Palaeogeogr. Palaeoclimatol. Palaeoecol.*, **487**, 278–295.

Mägdefrau, K. (1958) Die Kieselhölzer im obersten Oberkarbon des Kyffhäusergebirges. *Ber. Deut. Bot. Ges.*, **71**, 133–142.

Matysová, P., **Rössler, R.**, **Götze, J.**, **Leichmann, J.**, **Forbes, G.**, **Taylor, E.L.**, **Sakala, J.** and **Grygar, T.** (2010) Alluvial and volcanic pathways to silicified plant stems (Upper Carboniferous–Triassic) and their taphonomic and palaeoenvironmental meaning. *Palaeogeogr. Palaeoclimatol. Palaeoecol.*, **292**, 127–143.

McBride, E.F. (1963) A classification of common sandstones. *J. Sed. Petrol.*, **33**, 664–669.

Meissner, B. (1963) *Vorläufiger Bericht über einen Kristalltonstein aus dem Oberkarbon (Stefanien B/C) im Kyffhäuser*. Unpublished report, Zentrales Geologisches Institut Berlin, Berlin.

Meister, J. (1967) Sedimentpetrographische und lithologische Untersuchungen im Siles des Kyffhäusers. *Hall. Jb. Mitteldt. Erdgeschichte*, **9**, 75–92.

Mencl, V., **Matysová, P.** and **Sakala, J.** (2009) Silicified wood from the Czech part of the Intra Sudetic Basin (Late Pennsylvanian, Bohemian Massif, Czech Republic): systematics, silicification and palaeoenvironment. *N. Jb. Geol. Paläont. Abh.*, **252**, 269–288.

Mencl, V., **Bureš, J.** and **Sakala, J.** (2013) Summary of occurrence and taxonomy of silicified *Agathoxylon*-type of

wood in late Paleozoic basins of the Czech Republic. *Folia*, **47**, 14–26.

Miall, A.D. (1977) A review of the braided-river depositional environment. *Earth-Sci. Rev.*, **13**, 1–62.

Miall, A.D. (2006) *The Geology of Fluvial Deposits: Sedimentary Facies, Basin Analysis, and Petroleum Geology*. Springer, Berlin, Heidelberg, 582 pp.

Mickle, J.E. and **Barthel, M.** (1992) Psaronius-Stämme im Oberkarbon des Kyffhäuser? *Abh. Ber. Mus. Nat. Gotha*, **17**, 11–14.

Montañez, I.P. and **Poulsen, C.J.** (2013) The late Paleozoic Ice Age: an evolving paradigm. *Annu. Rev. Earth Planet. Sci.*, **41**, 629–656.

Moscariello, A., **Marchi, L.**, **Maraga, F.** and **Mortara, G.** (2002) Alluvial fans in the Italian Alps: sedimentary facies and processes. *Int. Assoc. Sedimentol. Spec. Publ.*, **32**, 141–166.

Nakamura, F. and **Swanson, F.J.** (1993) Effects of coarse woody debris on morphology and sediment storage of a mountain stream system in Western Oregon. *Earth Surf. Proc. Land.*, **18**, 43–61.

Nakayama, K. and **Ulak, P.D.** (1999) Evolution of fluvial style in the Siwalik Group in the foothills of the Nepal Himalaya. *Sed. Geol.*, **125**, 205–224.

Nakayama, K., **Fielding, C.R.** and **Alexander, J.** (2002) Variations in character and preservation potential of vegetation-induced obstacle marks in the variable discharge Burdekin River of north Queensland, Australia. *Sed. Geol.*, **149**, 199–218.

Nemec, W., **Porębski, S.J.** and **Steel, R.J.** (1980) Texture and structure of resedimented conglomerates: examples from Książ Formation (Famennian–Tournaisian), southwestern Poland. *Sedimentology*, **27**, 519–538.

Niklas, K.J. (1994) *Plant Allometry: The Scaling of Form and Processes*. University of Chicago Press, Chicago, 412 pp.

Noffke, N., **Gerdes, G.**, **Klenke, T.** and **Krumbein, W.E.** (2001) Microbially induced sedimentary structures – a new category within the classification of primary sedimentary structures. *J. Sed. Res.*, **71**, 649–656.

Opluštil, S. and **Cleal, C.J.** (2007) A comparative analysis of some Late Carboniferous basins of Variscan Europe. *Geol. Mag.*, **144**, 417–448.

Opluštil, S., **Martínek, K.** and **Tasáryová, Z.** (2005) Facies and architectural analysis of fluvial deposits of the Nýřany Member and the Týnec Formation (Westphalian D – Barruelian) in the Kladno-Rakovník and Pilsen basins. *Bull. Geosci.*, **80**, 45–66.

Opluštil, S., **Schmitz, M.**, **Cleal, C.J.** and **Martínek, K.** (2016a) A review of the Middle-Late Pennsylvanian west European regional substages and floral biozones, and their correlation to the Global Time Scale based on new U-Pb ages. *Earth-Sci. Rev.*, **154**, 301–335.

Opluštil, S., **Schmitz, M.**, **Kachlík, V.** and **Štamberg, S.** (2016b) Re-assessment of lithostratigraphy, biostratigraphy, and volcanic activity of the Late Paleozoic Intra-Sudetic, Krkonoše-Piedmont and Mnichovo Hradiště basins (Czech Republic) based on new U-Pb-TIMS ages. *Bull. Geosci.*, **91**, 399–432.

Opluštil, S., **Šimunek, Z.**, **Pšenička, J.**, **Bek, J.** and **Libertín, M.** (2017) A 25 million year macrofloral record (Carboniferous–Permian) in the Czech part of the Intra-Sudetic Basin; biostratigraphy, plant diversity and vegetation patterns. *Rev. Palaeobot. Palynol.*, **244**, 241–307.

Remy, W., **Remy, R.** and **Kampe, A.** (1961) Zur biostratigraphischen Stellung einiger rotgefärbter Sedimentkomplexe im Raume der Halleschen und der Mansfelder Mulde. *Monatsber. Dtsch. Akad. Wiss. Berlin*, **3**, 112–120.

Remy, W. and **Kampe, A.** (1961) Ausbildung und Abgrenzung des Autunien in der Halleschen Mulde. *Monatsber. Dtsch. Akad. Wiss. Berlin*, **3**, 394–408.

Roscher, M. and **Schneider, J.W.** (2006) Permo-Carboniferous climate: Early Pennsylvanian to Late Permian climate development of central Europe in a regional and global context. In: *Non-Marine Permian Biostratigraphy and Biochronology* (Eds S.G. Lucas, G. Cassinis and J.W. Schneider), *Geol. Soc. Spec. Publ.*, **265**, 95–136.

Rößler, R., **Philippe, M.**, **van Konijenburg-van Cittert, J.H.A.**, **McLoughlin, S.**, **Sakala, J.** and **Zijlstra, G.** (2014) Which name(s) should be used for Araucaria-like fossil wood? Results of a poll. *Taxon*, **63**, 177–184.

Rothwell, G.W., **Mapes, G.** and **Mapes, R.H.** (1997) Late Paleozoic conifers of North America: structure, diversity and occurrences. *Rev. Palaeobot. Palynol.*, **95**, 95–113.

Ruiz-Villanueva, V., **Díez-Herrero, A.**, **Ballesteros, J.A.** and **Bodoque, J.M.** (2014) Potential large woody debris recruitment due to landslides, bank erosion and floods in mountain basins: a quantitative estimation approach. *Riv. Res. Appl.*, **30**, 81–97.

Rygel, M.C., **Gibling, M.R.** and **Calder, F.J.** (2004) Vegetation-induced sedimentary structures from fossil forests in the Pennsylvanian Joggins Formation, Nova Scotia. *Sedimentology*, **51**, 531–552.

Schirmer, H. (1975) Lithologisch-geochemische Faziesuntersuchungen im Permosiles des nördlichen Saaletroges unter besonderer Berücksichtigung der Rotfärbung. Diploma Thesis, TU Bergakademie Freiberg, Freiberg, 116 pp.

Schneider, J.W. (1996) Biostratigraphie des kontinentalen Oberkarbon und Perm im Thüringer Wald, SW-Saale-Senke – Stand und Probleme. *Beitr. Geol. Thür. N. F.*, **3**, 121–151.

Schneider, J.W. and **Werneburg, R.** (2012) Biostratigraphie des Rotliegend mit Insekten und Amphibien. *Schriftenr. dt. geol. Ges.*, **61**, 110–142.

Schneider, J.W. and **Zajic, J.** (1994) Xenacanthiden (Pisces, Chondrichthyes) des mitteleuropäischen Oberkarbon und Perm – Revision der Originale zu Goldfuss 1847, Beyrich 1848, Kner 1867 und Fritsch 1879-1890. *Freib. Forsch.-H.*, **C 452**, 101–151.

Schneider, J.W., **Rößler, R.** and **Gaitzsch, B.** (1995) *Stratigraphy and Facies of the middle European continental Carboniferous and Permian. Excursion Guide, XIII.* International Congress on the Carboniferous and Permian. TU Bergakademie Freiberg, Freiberg, 31 pp.

Schneider, J.W., **Rößler, R.**, **Gaitzsch, B.**, **Gebhardt, U.**, **Kampe, A.** and **Breitkreuz, C.** (2005) Saale-Senke. *Courier Forschungsinst. Senckenberg*, **254**, 419–440.

Schneider, J.W., **Körner, F.**, **Roscher, M.** and **Kroner, U.** (2006) Permian climate development in the northern peri-Tethys area – The Lodève basin, French Massif Central, compared in a European and global context. *Palaeogeogr. Palaeoclimatol. Palaeoecol.*, **240**, 161–183.

Schneider, J.W., **Lucas, S.L.**, **Werneburg, R.** and **Rößler, R.** (2010) Euramerican Late Pennsylvanian/early Permian arthropleurid/tetrapod associations – implications for the habitat and paleobiology of the largest terrestrial arthropod. *Bull. N. M. Mus. Nat. Hist. Sci.*, **49**, 49–70.

Schneider, J.W., **Werneburg, R.**, **Rößler, R.**, **Voigt, S.** and **Scholze, F.** (2015) Example for the description of basins in

the CPT Nonmarine-Marine Correlation Chart Thuringian Forest Basin, East Germany. *Permophiles*, **61**, 29–35.

Schriel, W. and **Fulda, E.** (1926a) *Erläuterungen zur Geologischen Karte von Preußen und benachbarten deutschen Ländern. Blatt Kelbra*. Preußische Geologische Landesanstalt, Berlin, 56 pp.

Schriel, W. and **Fulda, E.** (1926b) *Erläuterungen zur Geologischen Karte von Preußen und benachbarten deutschen Ländern. Blatt Frankenhausen*. Preußische Geologische Landesanstalt, Berlin, 63 pp.

Schriel, W. and **von Bülow, K.** (1925) *Geologische Karte von Preußen und benachbarten deutschen Ländern*. Blatt Kelbra, Preußische Geologische Landesanstalt, Berlin.

Schriel, W. and **von Bülow, K.** (1926) *Geologische Karte von Preußen und benachbarten deutschen Ländern*. Blatt Frankenhausen, Preußische Geologische Landesanstalt, Berlin.

chweingruber, F.H., **Börner, A.** and **Schulze, E.-D.** (2006) *Atlas of Woody Plant Stems: Evolution, Structure and Environmental Modifications*. Springer, Berlin, Heidelberg, 229 pp.

Stikes, M.W. (2007) Fluvial facies and architecture of the Poison Strip Sandstone, Lower. Cretaceous Cedar Mountain Formation, Grand County, Utah Geological Survey Miscellaneous Publication 06-2, Salt Lake City, 111 pp.

Tabor, N.J. and **Poulsen, C.J.** (2008) Palaeoclimate across the Late Pennsylvanian-Early Permian tropical palaeolatitudes: A review of climate indicators, their distribution, and relation to palaeophysiographic climate factors. *Palaeogeogr. Palaeoclimatol. Palaeoecol.*, **268**, 293–310.

Tooth, S. and **Nanson, G.C.** (2000) The role of vegetation in the formation of anabranching channels in an ephemeral river, Northern plains, arid central Australia. *Hydrol. Process.*, **14**, 3099–3117.

Trümper, S. (2013) *Kartierung und Isotopenaltersdatierung der Mansfeld-Subgruppe im sachsen-anhaltinischen Anteil des Kyffhäusers unter Einbeziehung von Wismut-Bohrungen*. Unpublished mapping report, TU Bergakademie Freiberg, Freiberg, 176 pp.

Trümper, S., **Rößler, R.** and **Götze, J.** (2018) Deciphering silicification pathways of fossil forests: case studies from the Late Paleozoic of Central Europe. *Minerals*, **8**, 432.

Tyler, N. and **Ethridge, F.G.** (1983) Fluvial architecture of Jurassic Uranium-bearing sandstones, Colorado Plateau, western United States. *Spec. Publ. Int. Assoc. Sedimentol.*, **6**, 533–547.

Walch, J.E.I. (1771) *Die Naturgeschichte der Versteinerungen, 3. Teil*. Verlag Paul Jonathan Felßecker, Nürnberg, 235 pp.

Wallerstein, N.P., **Alonso, C.V.**, **Bennett, S.J.** and **Thorne, C.R.** (2001) Distorted Froude-scaled flume analysis of large woody debris. *Earth Surf. Proc. Land.*, **26**, 1265–1283.

Weiss, H.-J. (1998) Beobachtungen an Kieselhölzern des Kyffhäuser-Gebirges. *Veröff. Mus. Naturk. Chemnitz*, **21**, 37–48.

Weithofer, K.A. (1897) Der Schatzlar-Schadowitzer Mulden flügel des niederschlesisch-böhmischen Steinkohlenbeckens. *Jahrh. d. k. k. geol. Reichsanstalt*, **47**, 455–478.

Welber, M. (2013) Morphodynamics and wood dispersal in braided rivers. Doctoral Thesis, University of Trento, Trento, 169 pp.

Wooldridge, C.L. and **Hickin, E.J.** (2005) Radar architecture and evolution of channel bars in wandering gravel-bed rivers: Fraser and Squamish rivers, British Columbia, Canada. *J. Sed. Res.*, **75**, 844–860.

Zeh, A., **Gerdes, A.**, **Will, T.M.** and **Millar, I.L.** (2005) Provenance and Magmatic-Metamorphic Evolution of a Variscan Island-Arc Complex: Constraints from U-Pb Dating, Petrology, and Geospeedometry of the Kyffhäuser Crystalline Complex, Central Germany. *J. Petrol.*, **46**, 1393–1420.

Manuscript received 20 April 2019; revision accepted 5 November 2019

Supporting Information

Additional information may be found in the online version of this article:

Table S1. Calculation of wood compaction and original tree height. Green shading highlights samples, in which the calculated tree height equals to the original tree height; other samples provide minimum values. The red frame marks the sample with the largest calculated tree height.